Fluidic Diode Development and Optimization

Ryan Burnett, David Caso, Justin Tang
Department of Nuclear Engineering
University of California, Berkeley

Report UCBTH-10-002

May 14, 2010

ABSTRACT

The Pebble Bed Advanced High Temperature Reactor utilizes flibe as a liquid-salt coolant. As part of a passive decay heat removal, a flow element with anisotropic flow resistance is needed. For maximum reliability, this device is chosen to be a fluidic diode—a completely passive device with no moving parts. This type of device derives its name from its electrical component counterpart. Electrical diodes are devices that allow current to flow freely in one direction, but effectively block current from flowing in the opposite direction. This paper presents the design and fabrication of a vortex fluidic diode with a reduced length scale as well as an experiment that measures the performance of the prototypical fluidic diode. The experiment also compares variations in key geometrical parameters of the model fluidic diode to identify the most effective design for prototypical applications.

CONTENTS

1.0 INTRODUCTION

The Pebble-Bed Advanced High Temperature Reactor (PB-AHTR) is a Generation IV Small Modular Reactor (SMR) that offers a high power output (410MWe) while still having relatively small physical dimensions (Figure 1.1). This high core power density (20-30MW/m^3) is achieved through the use of TRISO coated fuel particles along with liquid fluoride salt coolants (flibe, $^7Li_2BeF_4$, as the primary coolant). The PB-AHTR uses an Intermediate Heat Exchanger (IHX) to remove decay heat during forced (normal operation) and natural circulation. It also uses DRACS Heat Exchangers (DHX) to remove additional decay heat during natural circulation (DRACS stands for Direct Reactor Auxiliary Cooling System and is discussed in further detail in Section 2.0). It is necessary to restrict coolant flow through the DHXs during forced circulation for power operation and allow it to flow in the opposite direction under natural circulation for decay heat removal. It is preferable to use a use a device such as a fluidic diode for this function due to the fact that it has no moving parts and therefore very low probability of having a mechanical failure that would force an unscheduled reactor shutdown.

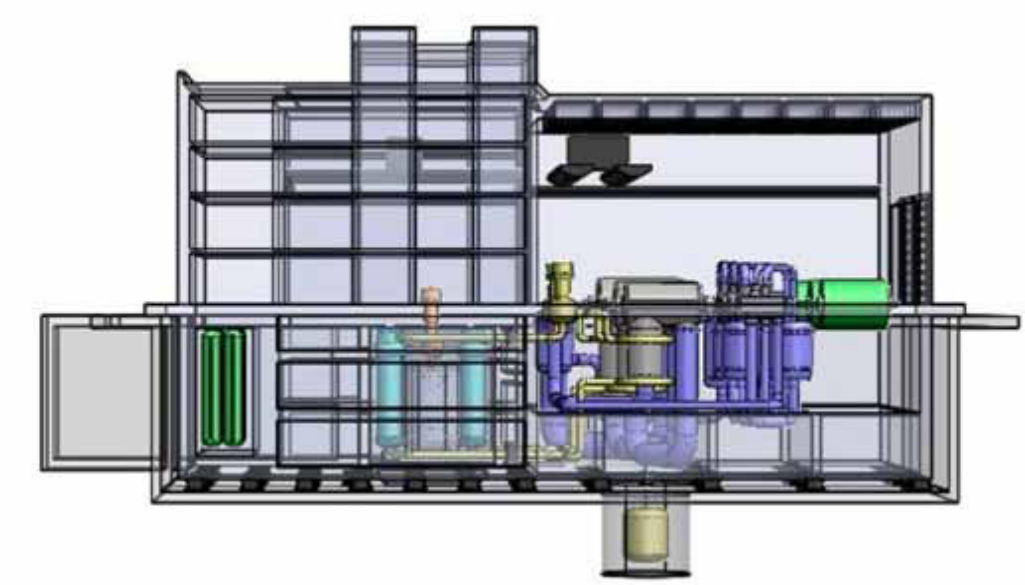

Fig. 1-1 PB-AHTR 3-D power plant model.

A fluidic diode is a device, with no moving parts, in which fluid experiences a high flow resistance in one direction and a low flow resistance in the other direction. This concept originated in the 1930's from the work of Thoma, Zobel and others on vortex throttles and diodes at the Munich Technical University. This work was incorporated into the broader field of fluid dynamics until 1959 when it was expanded upon and identified as a specific sub discipline of fluid dynamics called fluidics at the Harry Diamond laboratory in Washington DC. The term fluidics is now used to describe the study of any fluid control element with no moving parts. There are three main fluidic diode prototypes that exist today, the scroll diode, the fluidic rectifier diode and the vortex diode (or Zobel diode). The effectiveness of these fluidic diodes is measured by their diodicity. Diodicity is the ratio of the pressure differential in the direction of high flow resistance to

the pressure differential in the direction of low flow resistance, at the same flow rate. For typical designs the scroll diode has a relatively low diodicity in comparison to the rectifier or vortex diodes (Figure 1.2). The vortex diode has been tested for diodicities as high as about 60 with higher diodicities thought to be achievable through optimization of diode design and axial and tangential flow conditions [1].

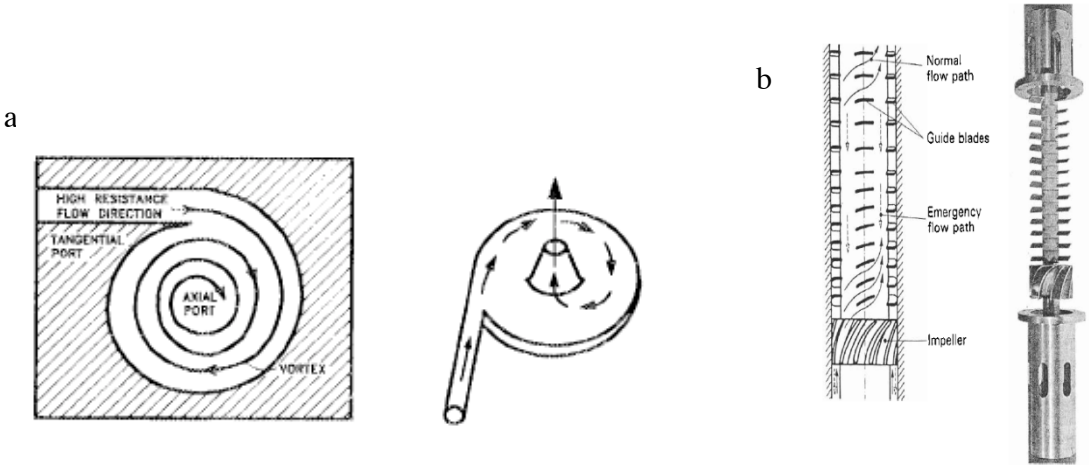

Fig. 1-2 (a) Shows a vortex diode with fluid flowing in the tangential port, which is the high resistance direction [2]. (b) Shows a rectifier diode design [3].

There are many benefits to using fluidic diodes for applications in nuclear reactors. One important benefit is that because there are no moving parts in the fluidic diode the risk of a mechanical failure of the fluid control element is greatly reduced. This is an important advantage since failed mechanical elements in a reactor may lead to unscheduled reactor shutdowns which make up a large portion of the cost associated with reactor operation. Fluidic diodes can also be useful in the event of a reactor accident. Due to the fact that the diode restricts flow in one direction, fluid would leak out in only one direction in the event of a broken pipe. For these reasons fluidic diodes are already widely used in the nuclear industry. Vortex diodes are being used in British Advanced Gas-Cooled Reactors (AGRs), as well as in designs for Safe Integral Reactors (SIRs), which are a type of PWR developed by Combustion Engineering and Rolls Royce and Associates. Fluidic diodes are also widely used in the oil and chemical industries [2].

For our experiment we had to choose between the fluidic rectifier diode and the vortex diode. A brief description of each is given below. The fluidic rectifier utilizes the principals of resistance and turbulence to create the diode effect. The basic principal of a rectifier diode is to impart a swirl on the fluid flowing in the direction of high resistance by having blades axially attached to a cylinder that become gradually more perpendicular to the cylinder as the fluid travels towards the exit at the top of the device. The slits between the blades at the outer walls ensure that fluid flowing in the low resistance direction experiences minimal flow reduction. There is not much experimental data currently available for fluidic rectifiers, but in a report from Oakridge National Laboratories [2] the rectifier diode is said to be a lower-performance device due to its low diodicity. However some theories suggest that higher diodicities could be achieved if the rectifier design was optimized. Due to the time constraints and advanced design and

experimental procedures that would be required to further explore the rectifier diode we chose the more proven vortex diode for our experiment. The vortex diode is also superior to the scroll diode in terms of its achievable diodicity as stated above.

The vortex diode is composed of a disc shaped chamber with rounded interior edges. An image of this diode can be seen in Figure 1 below. There are two ports for fluid to flow into or out of the chamber, one is tangent to the disc and the other is axial to the disk. Fluid going into the diode through the tangential port will experience momentum loss as it spirals towards the center of the disc. High centrifugal forces develop that resist fluid flow. This causes a solid body rotation effect on the fluid at the center of the chamber which causes a reduction in pressure for the flow leaving the chamber through the axial port. If flow is reversed and it enters through the axial port it will lose very little momentum as most of the flow will disperse out radially and flow out of the tangential port effectively seeing only a small resistance comparable to that of a 90 degree pipe bend. Simulations of the fluid particle path lines for the vortex diode in both the forward and reverse directions were performed by the Industrial Flow Modeling Group at National Chemical Laboratory and can be seen in Figure 1.3 below.

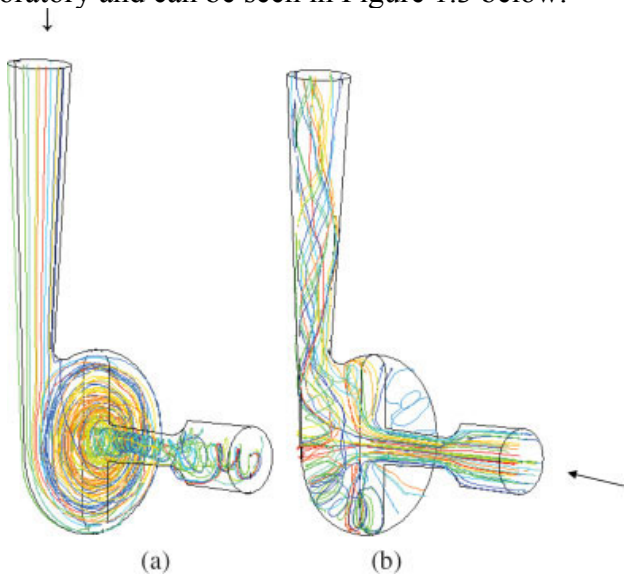

Fig. 1-3 Typical path lines of the fluid in a 125 mm vortex diode at inlet velocity of 0.423m/s for the case of (a) reverse flow, and (b) forward flow situations [1].

The predicted diodicity for such a design is thought to be higher than the scroll or rectifier diodes and has a significantly simpler design and experimental setup. There was also more information available on the design variation and the fluidic properties associated with the vortex diode design. We used the results from a study on the German vortex diode conducted by the Industrial Flow Modeling Group (IFMG) at National Chemical Laboratory in Pune India as the basis of our experiment [4]. In their experiment the IFMG studied the dependence of the diodicity of a vortex diode on the diode geometry, diode size, aspect ratio, nozzle configuration, and Reynolds number. In this experiment it was determined that the Reynolds number greatly increased the diodicity up to a cutoff were the diodicity then remained relatively constant. The

diodicities found in these experiments were around 50-60 for a larger diode chamber and Reynolds number. Our goal in this experiment was to attempt to find an optimum diode design for use in the PB-AHTR reactor by measuring the diodicity while varying the dimensions of the diode chamber as well as varying the dimensions of the axial port and the inlet conditions for reverse flow at the tangential port. The last parameter was varied in an attempt to increase momentum transfer in the high resistance direction that we predict may give higher diodicity.

For this experiment it was also important to identify an optimum design for a diode specifically for use in the Pebble Bed Advanced High Temperature Reactor (PB-AHTR). The PB-AHTR may require sufficient diodicity at relatively low Reynolds number. It is therefore important to determine the maximum diodicity achievable with a fluidic diode for the flow rates as well as the coolant density and Reynolds number seen in the PB-AHTR. The experiment was performed using water instead of the reactor coolant flibe. As a result we scaled the geometric dimensions as well as the Reynolds and Euler numbers for our experiment. Further discussion of the scaling done for our experiment can be found in Section 4.2.

2.0 APPLICATION TO PB-AHTR

Following shutdown of the reactor, the PB-AHTR is designed to remove decay heat through the Intermediate Heat Exchangers (IHX) under natural or forced circulation. The PB-AHTR also has a Direct Reactor Auxiliary Cooling System (DRACS) that can remove approximately 2% of the reactor's total thermal power using natural circulation. When in a loss of forced circulation (LOFC) transient, buoyancy forces will move the coolant through the DRACS Heat Exchangers (DHX) passively and remove heat via transfer to a DRACS salt loop and ultimately via air cooling. The DHX units are shell-and-tube, one-pass vertical exchangers with disk-doughnut baffle pairs and provide fully passive heat removal by air-cooling. Table 1 below shows important dimensions and values associated with the current DHX design. The values in Table 1 were obtained through contact with Dr. Hyunjin Lim, a post doctoral scholar and Christhian Galvez, a graduate student working on the PB-AHTR at the University of California, Berkeley. Under forced circulation, power operation, bypass flow through the DRACS loop is undesirable as this reduces the fraction of flow going through the core and increases the temperature of the flow exiting the core and the potential for cyclic thermal stresses on components near where the cold DHX flow and hot core flow mix before entering the reactor hot leg. The shell side of the DHX is connected to the primary loop and is isolated by a fluidic diode. The fluidic diode will minimize bypass flow under forced circulation (e.g. normal operation), and provide low flow-resistance under natural circulation (e.g. LOFC transients). This will provide high efficiency under normal operation and maximum passive decay heat removal under accident scenarios.

Table 2.1 Critical DHX Parameters

Number of required units	Eight
Heat transfer rate per unit (MWth)	2.25
Primary salt (hot side, shell)	flibe
Secondary salt (cold side, tube)	flinabe
Structure Material	Hastelloy alloy
Thermal conductivity, tube material (W/ m^2 °C)	20.08
Inlet temperature of primary salt, shell side (°C)	704.0
Outlet temperature of primary salt, shell side (°C)	600.0
Inlet temperature of secondary salt, tube side (°C)	510.0
Outlet temperature of secondary salt, tube side (°C)	610.0
Mass flow rate of flibe, shell side (kg/sec)	9.06
Mass flow rate of flinabe, tube side (kg/sec)	10.98
DHX approx. length (m)	2.6
Nominal DHX diameter (m)	0.53
Total flinabe volume in tubes (m^3)	0.68
Total heat transfer area based on tube O.D (m^2)	55.37
Tube side avg. heat transfer coeff. (W/ m^2 °C)	680.6
Shell side avg. heat transfer coeff. (W/ m^2 °C)	4376.3
Pressure drop in shell side (bar)	0.005
Pressure drop in tube side (bar)	0.028

The fluidic diode should ideally have a high diodicity (which is the ratio of pressure drop for the forward flow to the pressure drop for an equal flow in the reverse direction). In addition to a high diodicity, the pressure drop across the fluidic diode in the low flow-resistance direction must only be a few percent of the total forced-circulation pressure drop across the core. For instance, a high diodicity diode that performs very well is not applicable in our design if it inhibits natural circulation flow.

The purpose of finding the diodicity of the models is two-fold: the first reason is to attempt to identify the optimal design of a vortex diode for use in the PB-AHTR. The second goal of finding the diodicity of these designs is for validating input data on Reactor Excursion Leak Accident Program (RELAP5-3D) simulations for the PB-AHTR. The RELAP5-3D code has been used to simulate critical transients—loss of heat sink (LOHS) and loss of forced convection (LOFC) accidents with and without reactor SCRAM—to show that the peak fuel temperature does not exceed design bases. The final values calculated may be sensitive to the performance of the fluidic diode. Currently the code assumes that the diode has a ratio of 100:1 in loss coefficient. The experimentally obtained performance from the vortex diode will be used to determine whether or not this assumption is reasonable [5].

3.0 VORTEX DIODE DESIGN AND FABRICATION

The vortex fluidic diode is composed of three major components: the axial port, tangential port, and vortex chamber. Our diode is designed to be modular so all three components can be switched and changed so different combinations of the components can be tested for performance. In our study we are not varying the geometry of the tangential port, but we will be making measurements for various axial ports and vortex chambers. Figure 3-1 shows the diode assembly and all the parts needed for our experiment such as diode chamber, tangential port and axial port as well as their key dimensions.

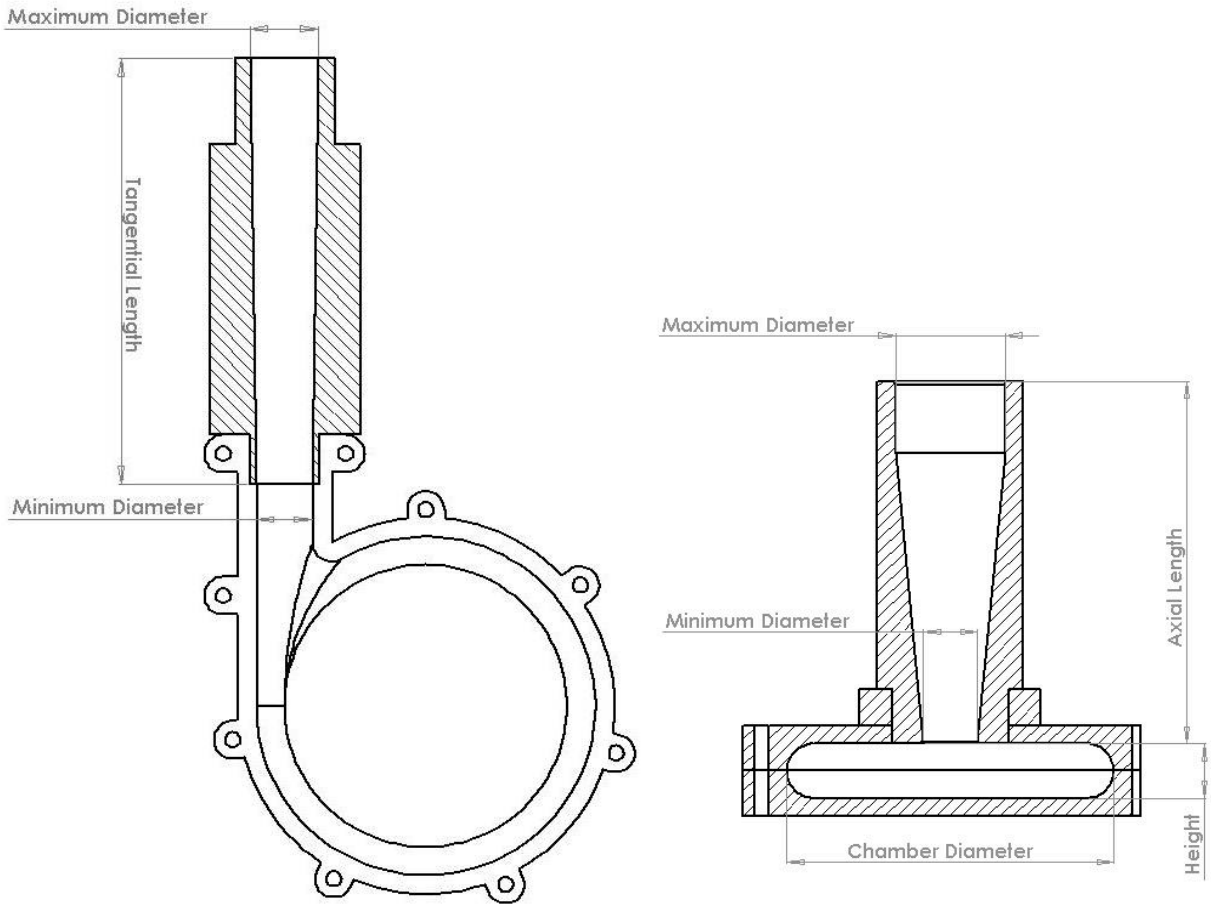

Fig. 3-1 Schematic of the top and side view of the diode assembly.

The interior of the vortex chamber is a torus-like shape. The walls are curved with a radius that is half of the chamber height. Near the tangential port neck, the sharp edge at the exit has a smooth fillet to aid in the low-resistance flow direction. Figure 3-2 shows the interior of the vortex chamber.

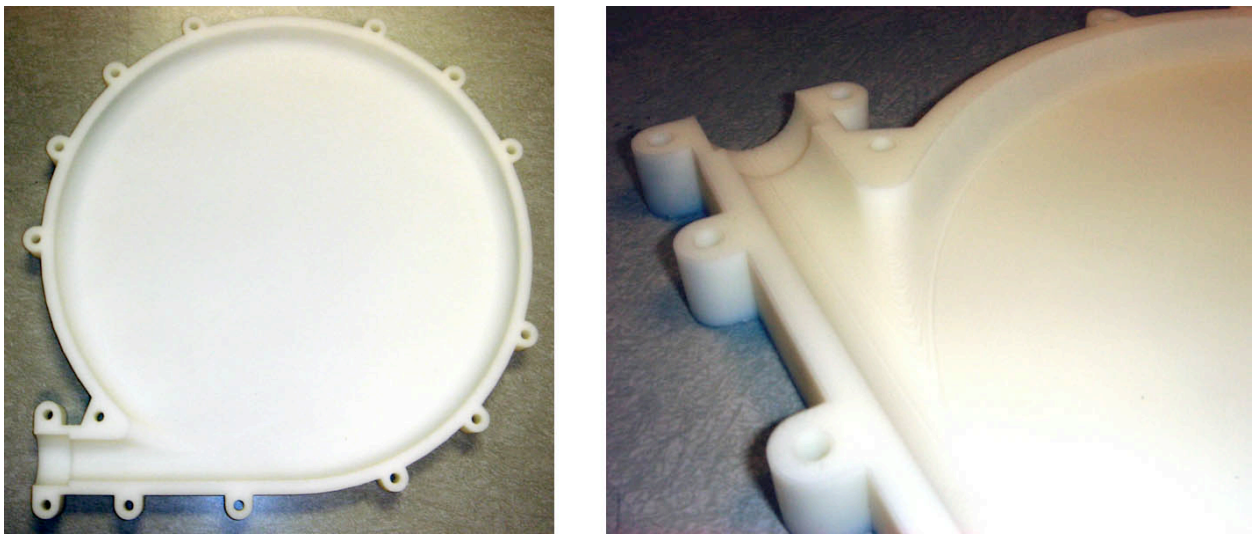

Fig. 3-2 Interior photos of the vortex chamber before applying smoothing methods to the surface.

The vortex chamber is responsible for inducing the swirling vortex. As the water jet first impacts the wall of the vortex chamber, there is a free swirling jet that traverses the perimeter of the chamber. As the fluid moves inward towards the center, turbulent eddies transfer momentum radially and at high Reynolds number the flow approaches rigid-body rotation. In this rigid-body rotation, the fluid dissipates kinetic energy through frictional losses and the flow out through the axial port is impeded. Where this transition occurs will be an important factor in how much flow is impeded in the high-resistance direction. Equation 3.1 defines the aspect ratio, α, as the ratio between the diameter of the vortex chamber and the height of the chamber.

$$\alpha = D_c/h \qquad (3.1)$$

There is some tradeoff: as the aspect ratio increases, the more losses accumulate for flow in the low-resistance direction. Figure 3-3 shows a comparison between two vortex chambers.

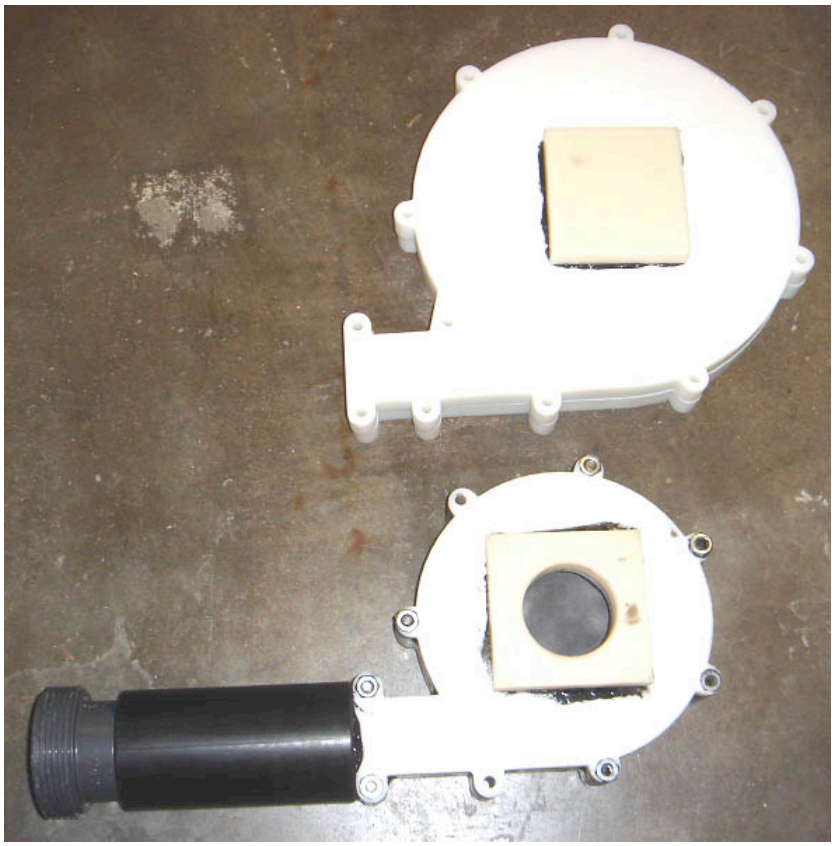

Fig. 3-3 Two vortex chambers with different aspect ratios, $\alpha = 9$ (top) and $\alpha = 6$ (bottom).

Varying the aspect ratio will change where this transition occurs. In the study by the Indira Gandhi Center for Atomic Research, the diodicity depended strongly on the aspect ratio of the vortex chamber [4]. Since our study will not be varying the tangential chamber, the height will remain constant and the vortex chamber diameter will be varied to achieve a range of aspect ratios.

In order to create the diode chamber it was necessary to look at different fabrication possibilities and how time-consuming and affordable they were. After comparing many methods, the 3D printing fabrication process became attractive for the low cost and fast fabrication time. ABS plastic is used as a build material which is heated to 65 °C. Material directed through a small nozzle and is deposited as a string. The part is created by successive cross-sectional layers one on top of the other until the part is completed. 3D printing requires dissolvable support material to create hollow spaces or to support thin walls. Support material contributes the cost of the part.

For our diode design it was decided to construct the diode in two pieces to be chemically bonded. The two-piece construction gives access to the inside surface of the vortex chamber. Tabs were added to allow the two halves to be bolted together.

A square piece of ABS plastic was glued on top of the diode to increase the wall thickness for threads. The axial port would screw into this top hole. While trying to drill and tap the hole for the axial port, the small diode suffered splintering of the layers on the inside surface. The successive layers of ABS, characteristic to the 3D printing process, were sheared off from the lateral motion of the drill. To remedy this problem a small layer of ABS cement was applied to the damaged surface and then sanded down to have a smooth surface. This process was also done for the next two diodes before drilling and tapping the axial hole, which prevented the splintering.

The tangential port hole also suffered some splitting in the process of tapping the hole for the tangential port. The threads traversed several layers of the ABS material, so there were layers that were not supported. The decision was made to glue the tangential port and vortex chamber together to avoid any leakage between the two parts.

The axial port's interior geometry is a linear taper between a minimum and maximum diameter. The minimum diameter is the side directly attached to the vortex chamber while the maximum diameter is the side that is furthest from the vortex chamber. There is a rounded edge at the exit. The gentle taper is to diffuse the flow exiting the diode in the high-resistance direction and to nozzle the flow in the low-resistance direction. The rounded edge minimizes any turbulent eddies from forming when flow enters the axial port in the low-resistance direction. For fluid entering the port from the side, a sharp edge would instigate turbulence. While keeping the maximum diameter constant, the minimum diameter is varied to see the effect on performance. The nominal value for the minimum diameter is equal to the height, h, of the vortex chamber. Figure 3-4 shows a comparison between some of the axial ports.

Fig. 3-4 Axial port comparison for a fixed length. The middle port is the nominal size. Ports with minimum diameter smaller and larger than the nominal will be tested. All three ports have the same outer diameter so they can be screwed into the tops of the vortex chambers.

Similar to the axial port, the tangential port has a linear taper from the vortex chamber height to a maximum diameter. The purpose of the tangential port is to nozzle the flow in

the high-resistance direction. The taper increases the velocity of the jet to set up a stronger swirling vortex. In the low-resistance direction, the gentle taper helps with pressure recovery since the entrance to the vortex chamber has the smallest diameter.

The axial and tangential ports were constructed from a stock piece of 5.08-cm (2.0 inch) diameter ABS plastic. The fabrication for these pieces was done in the student machine shop using a lathe to create the desired bored and linear taper for both parts. It was important to have a flush surface between the diode, axial and tangential port for smooth transitions.

4.0 DIODE PERFORMANCE EXPERIMENT

4.1 Scaling Arguments

For the fluidic diode experiment, we are concerned with momentum transport and mass continuity. The Navier-Stokes equation can be non-dimentionalized into the Strouhal, Euler, Froude, and Reynolds numbers as seen in equation 4.1 for characteristic length, D, and characteristic velocity, u [6].

$$\vec{V}^* = \vec{V}/u \qquad P^* = \frac{P - P_\infty}{P_0 - P_\infty} \qquad t^* = \frac{t}{D/u} \qquad \vec{g}^* = \vec{g}/g \qquad \vec{\nabla}^* = D\vec{\nabla}$$

$$[St]\frac{\partial V^*}{\partial t^*} + (\vec{V}^* \bullet \vec{\nabla}^*)\vec{V}^* = -[Eu]\vec{\nabla}^* P^* + \frac{1}{[Fr]^2}\vec{g}^* + \frac{1}{[\mathrm{Re}]}\nabla^{*2}\vec{V}^* \qquad (4.1)$$

We choose the characteristic length to be the pipe diameter. The characteristic velocity is chosen to be the velocity far upstream from our system. In the experiment it is the velocity at the supply line and can be measured with a flow meter. The far upstream pressure, P_∞, is chosen to be atmospheric pressure. In the model, there is a free surface above the axial port of the diode where the pressure is atmospheric. In the prototypical system, the top of the axial port is connected to the DHX which has a free surface as well.

For this experiment, we are only interested in steady state conditions so the Strouhal number drops out of our dimensional analysis. We are also not concerned with natural circulation so the Froude number is dropped as well. By conserving both the Reynolds and Euler numbers (defined in equations 4.2), dynamic similarity is maintained.

$$\mathrm{Re} = \frac{\rho D v}{\mu} \qquad Eu = \frac{P}{\rho v^2} \qquad (4.2)$$

Equation 4.1 applies to both the prototype and the model. If we choose to match the Reynolds number and the Euler number, the non-dimentionalized equations become identical for the model and the prototype. This assures that dynamic similarity is achieved

where the observed phenomena in our model is the same as what we would observe in the prototype. Equations 4.3 shows the matching of Reynolds and Euler numbers. Here the subscript 'm' and 'p' denotes the model and prototype respectively.

$$\frac{\mathrm{Re}_m}{\mathrm{Re}_p} = \frac{Eu_m}{Eu_p} = 1$$

$$\left(\frac{\rho_m}{\rho_p}\right) \bullet \left(\frac{L_m}{L_p}\right) \bullet \left(\frac{V_m}{V_p}\right) \bullet \left(\frac{\mu_p}{\mu_m}\right) = \left(\frac{\Delta P_m}{\Delta P_p}\right) \bullet \left(\frac{\rho_p}{\rho_m}\right) \bullet \left(\frac{V_p}{V_m}\right)^2 = 1 \qquad (4.3)$$

$$V_m \Big/ V_p = \left[\left[\left(\frac{\rho_m^2 \Big/ \rho_p^2}{\mu_m \Big/ \mu_p}\right)\right] \bullet \frac{L_m}{L_p}\right]^{-1/3}$$

We assume that the pressure drop across the diode for model is equal to that of the prototype. For this experiment, water at room temperature was chosen as the simulant fluid. Numerically the ratio of the densities squared to the ratio of the dynamic viscosities for water and flibe as the model and prototypical fluids is approximately 2. By choosing a 50% length scale for the model, the model flow velocity is matched to the prototype flow velocity.

The performance of the fluidic diode should be measured over a range of Reynolds numbers due to the various flow conditions that need to be accommodated. The flow rates under normal power operation are much different compared to abnormal conditions. While the geometry of the supply lines for the experiment is fixed, we are able to cover a range of Reynolds numbers by varying the flow rate.

For normal power operation, fluid is expected to move in the high-resistance direction. The fluidic diode's function is to minimize bypass flow though the DHX units. We expect the flow condition to potentially reach high Reynolds numbers as high as 45,000. There are several reactor transients in which fluid is still forced through the high-resistance direction, but the coolant rises in temperature. Table 4.1 displays temperature-dependent thermophysical properties of flibe. Under such transients, the maximum Reynolds number will be approximately 55,000.

Table 4.1 Thermophysical properties of prototypical coolant and simulant fluid.

	Flibe	Water
Density	1987.0 kg/m^3 (600˚C) 1962.5 kg/m^3 (650˚C) 1913.7 kg/m^3 (750˚C)	1000.0 kg/m^3 (25˚C)
Dynamic viscosity	8.56 E -03 kg/ m·s (600˚C) 6.78 E -03 kg/ m·s (650˚C) 4.56 E -03 kg/ m·s (750˚C)	8.925 E -04 kg/m·s (25˚C)

When the reactor loses forced circulation capability, the flow reverses through the core and coolant moves through the low-resistance direction of the fluidic diode. In this direction it is necessary to minimize resistance to maximize flow and minimize temperature drop through the eight DHX units that remove decay head from the core.

By fixing the length scale between the prototypical and model (in this case, pipe diameter), a range of model flow velocities that are representative to the prototypical flow velocities can be applied to each diode assembly. Our measured pressure drops for the model will reflect the pressure drops in the prototype.

4.2 Experimental Setup

For our experiment we placed the diode in a 44.45cm X 29.21cm X 48.26 cm tank shown in figure 4-1 below. We placed an acrylic plate at the bottom of the tank and bolted the diode to this plate using three screws. The screws went through three of the flanges that were built into the diode for the purpose of bolting the two halves together. This secured the diode from moving due to buoyancy forces or inertial forces from the water inside the diode.

To give the fluid more initial momentum as it entered through the tangential port in the reverse flow direction we attached a nozzle to each of the diodes we tested. This nozzle was about 14.35 cm long with a tapered angle of down to the minimum diameter just at the axial port. The nozzle which is referred to in this paper as the tangential port was glued onto each of the diodes. The male end of a 1" union was glued to the end of the tangential port and attached to a bulk head at the bottom of the tank.

Fig 4-1 Top view of the fluidic diode (α=6) in the tank under reverse flow conditions at a low flow rate.

In addition to giving the fluid greater momentum at the tangential inlet we also tested the effects of imparting an initial turbulence on the fluid traveling in the high resistance direction just before it entered into the tangential port. We did this by using unions to remove a 30 cm section of pipe located just outside of the lower bulk head of the tank and replacing it with a series of four elbows.

We used PVC piping and ball valves to control the direction of the flow. Our experiment was designed so that it could be run in the forward and reverse directions. A schematic of this loop can be seen below (Fig. 4-2). Forward flow is run by closing valve 3 and opening valves 2 and 4. In this case water will flow into the tank through the upper bulk head and then down into the diode through the axial port. The water then flows out through the tangential port to the drain. For reverse flow valves 2 and 4 are closed and valve 3 is opened. Fluid then flows into the diode through the tangential port and then out of the diode and into the tank through the axial port. Fluid then fills the tank until it reaches the upper bulkhead where it then flows out to the drain. To avoid siphoning we adjusted our drain lines to be the same height as the piping coming from the lower bulkhead of the tank.

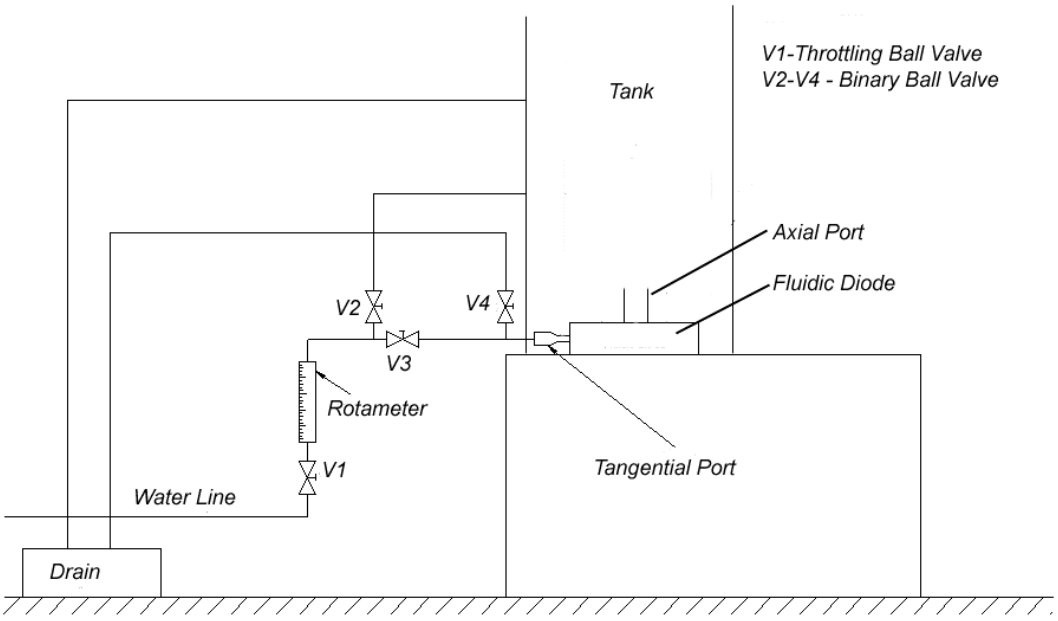

Fig. 4-2 Loop Schematic for fluidic diode scaled experiment

The pressure drop across the diode in the forward and reverse directions was measured using the relative pressure difference between two manometers. One manometer was connected to the pipe just outside the lower bulkhead. The other manometer was connected to the tank about halfway between the upper and lower bulkheads. These manometers were then attached to a vertical board for support. We then attached a tape measure along side of the manometers and used a level to get the most accurate reading possible. Due to practical height restrictions we could not use the manometers to

measure the high pressure in the reverse direction at high flow rates. It was therefore necessary to also connect a pressure gauge to the piping just before the tangential port on the outside of the tank. We also connected a tube to the high pressure manometer in the reverse direction to drain excess water at high flow rates. We used the manometer to calibrate the pressure gauge. To do this we adjusted the flow rate so that we got a reading of 6.89 KPa on the pressure gauge and measured the pressure head reading on the manometer at that flow rate. In this way we determined that 1 psi on our pressure gauge equated to approximately 31" on our manometers. A picture of our entire experimental loop is shown in Fig. 4-3 below.

Fig. 4-3 Picture of experimental loop setup for high resistance flow direction.

For our experiment we varied the diameter of the axial port, the aspect ratio of the diode, and the inlet conditions just before the flow enters the tangential diffuser in reverse flow. To determine the effect that the diameter of the axial port has on diodicity we constructed three different axial ports all with a length of 12.7 cm. The axial ports were tapered at an angle of about 5° down to their smallest diameter, which was attached to the axial port on the diode. To vary the aspect ratio we constructed three diodes with different diameters but equal height. We used a series of elbows that can be seen in Fig. 4-3, as well as a straight section of pipe to determine the effect of giving the fluid initial turbulence as it enters the tangential port. These test parameters are discussed in Section 4.3.

4.3 Varied Parameters

In this experiment, several parameters were chosen to observe the effect on the performance of the vortex diode. Table 4-1 summarizes the various parameters associated with the axial port that were varied.

Table 4-1 Axial Port Dimensions

	Axial Port #1	Axial Port #2	Axial Port #3	Axial Port #4
Length	12.7 cm	12.7 cm	12.7 cm	6.35 cm
Minimum Diameter	1.27 cm	1.905 cm	2.54 cm	1.905 cm
Maximum Diameter	3.81 cm	3.81 cm	3.81 cm	3.81 cm

Various minimum diameters were tested to observe the effects on pressure losses in both high and low resistance paths and their respective impact on diodicity.

The aspect ratio of the vortex chambers was also varied. By keeping height constant and varying the diameter of the chamber, a range of aspect ratios were achieved. Table 4-2 summarizes key parameters that were used for the vortex chamber.

Table 4-2 Vortex Chamber Dimensions

	Vortex Chamber #1	Vortex Chamber #2	Vortex Chamber #3
Height	1.905 cm	1.905 cm	1.905 cm
Chamber Diameter	11.43 cm	17.145 cm	22.86 cm
Aspect Ratio	6	9	12

In addition to these parameters, two different inlet conditions were tested. One inlet condition used a straight 1” PVC pipe that connects to the tangential port of the vortex diode. The second inlet condition directs flow through four elbow fittings in series before entering the tangential port.

The first test sequence holds the vortex chamber and inlet condition constant and testing the axial ports 1-3. This provides a direct comparison of the effects of changing the minimum diameter on the axial port.

The second test sequence holds the axial port and inlet conditions constant and testing vortex chambers 1-3. This provides a direct comparison of the effects of changing the aspect ratio on the vortex chamber.

The third test sequence holds the vortex chamber constant and the inlet condition constant and testing axial port #2 and #4. This provides a direct comparison of the effects of the axial port height (since the minimum and maximum diameters are equal for axial port #2 and #4).

The fourth test sequence holds the vortex chamber and axial port constant and varying the inlet condition. This provides a direct comparison of the effects of the inlet condition.

5.0 EXPERIMENTAL RESULTS

5.1 Data Analysis

For our experiment we measured the pressure drop across the diode while varying the diameter of the diode, the diameter of the axial port, the height of the axial port and the inlet conditions for flow going into the diode in the high resistance direction. We took measurements of the pressure before and after it entered the diode in both the high flow resistance direction and low flow resistance direction. The ratio of the pressure drop across the diode in the high resistance direction ($\Delta \mathbf{P}_H$) and the low resistance direction ($\Delta \mathbf{P}_L$) is called the diodicity and is referred to as D from this point forward.

We measured $\Delta \mathbf{P}_H$ and $\Delta \mathbf{P}_L$ for increasing flow rates. We did this to determine how the diodicity changed with increasing Reynolds number, which increases proportionally to flow rate. Determining diodicity through a range of Reynolds numbers is important because not only can we determine how diodicity changes with flow rate for the given set of parameters, we can also see the effects that a variable Reynolds will have on the system. This is important because the Reynolds number in the reactor will vary. The lowest flow rate we were able to accurately measure with our rotameter was 1.5 gpm. We could not take accurate measurements at this low of a flow rate however, because when we used the 12.7 cm long axial ports, the water level to maintain a steady state flow through the diode would need to fall lower than the height of the axial port. The minimum flow rate at which we could get accurate diodicity measurements varied with the diode diameter, axial port diameter, axial port height and the high resistance inlet flow conditions. For the small diode ($\alpha = 6$) with axial port 1 and laminar inlet flow conditions for the high resistance direction the minimum flow rate for which we were able to accurately measure $\Delta \mathbf{P}_L$ was 3 gpm. The maximum flow rate for which we could accurately measure diodicity was also was also limited due to inaccuracies in the low resistance direction. This occurred because the pressure head required for the flow rate to reach steady state was high than the height of our tank. This has the simple solution of getting a taller tank. There are also a number of other ways to modify the experiment to allow for accurate measurements at higher Reynolds numbers (see section 6.1). The maximum flow rate for the conditions listed above was 5 gpm. The increments of flow rate measurements on our rotameter also limited the number of flow rates within this range (3-5gpm) that we could take accurate measurements of flow rate. We therefore could only adjust the flow rate by increments of 0.5gpm. Due to the issues discussed above we were only able to collect a limited amount of diodicity measurements for each diode setup (measurements taken range from 5-7). We therefore recorded the $\Delta \mathbf{P}_H$ and $\Delta \mathbf{P}_L$ for the conditions specified above. A graph showing the diodicity with increasing

Reynolds number for the small diode with axial ports 1, 2 and 3 attached can be seen in Figure 5-1 below.

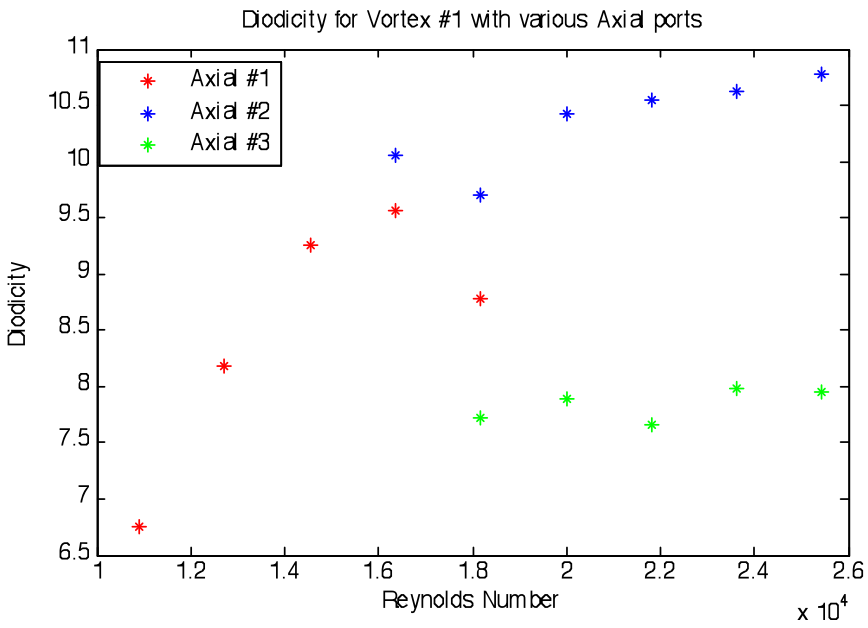

Fig. 5-1 Diodicity with respect to Reynolds number for small diode with axial ports 1, 2 and 3.

As can be seen in Figure 5-1 the diodicity when using axial port 2 was better than the diodicity when using axial port 3 for Reynolds numbers ranging from 1.8 x10^4 to 2.6 x10^4. It also appears from the data that the diodicity measured with axial port 2 would greater than that measured with axial port 1. This can only be inferred from the trend of the data points above because the range of Reynolds for the axial point 1 and 2 were not the same. This result makes physical sense, because although the pressure drop with axial point 2 in the high resistance direction was not as large as the that with axial port 1, and the pressure drop in the low resistance direction was not as low as that measured with axial port 3 it is the ratio of these two pressure drops that is important. The diameter of axial port 1 apparently offers the best balance of the three axial ports in our experiment. This diameter was 150% the diameter of the tangential inlet port. It is therefore possible to predict that better diodicity may be achieved when making the axial port diameter 150% the length of the tangential port diameter.

Another parameter that we varied in our experiment was the diode aspect ratio. This ratio is determined by the diameter of our diodes since we kept the height of the three diodes constant. The aspect ratios we used were 6, 9 and 12; referred to here as the small, medium, and large diodes respectively. We measured the diodicity of these different sized diodes with varying flow rates as described above. The results are shown in Figure 5-2 below.

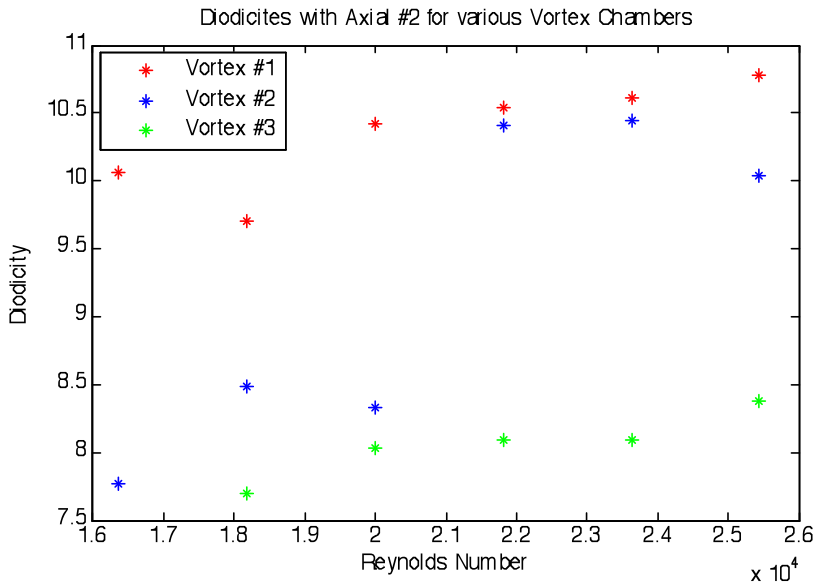

Fig. 5-2 Diodicity with respect to Reynolds number for small, medium, and large diodes with axial port #2.

It can be seen in Fig. 5-2 that the small diode had larger diodicities than the medium and large diodes for the measured range of Reynolds numbers. This was a predictable result when looking at a similar experiment done by the Industrial Flow Modeling Group [4] on the German Vortex Diode. In this experiment the maximum diode aspect ratio was 6. In their study the Industrial Flow Modeling Group found that the diodicity increased as the aspect ratio was increased from 4 to 6. This is shown to be the point where the aspect ratio was the optimum value. At larger values the diodicity would begin to decrease due to the fact that the fluid would laminarize prior to forming the rigid body rotation at its center. This seemed to be the case with the larger diodes as the diodicity grew smaller as the aspect ratio increased. It cannot be concluded from this data or past experiments that the optimum diode aspect ratio is 6. However it can be concluded that the maximum diodicity at relatively small Reynolds numbers (1.1-2.6 x 10^4) occurs when the aspect ratio is somewhere in the range from 6 – 9.

We also tested the effects of the diode axial exit port height on diodicity. For this we used the used the small diode and axial port 2. We also used a shorter axial port called axial port 4 with the same diameters as the axial port 2. We performed the same measurements for the two ports as was done in the previous diodes setups described above. The results of this experiment are shown in Figure 5-3 below.

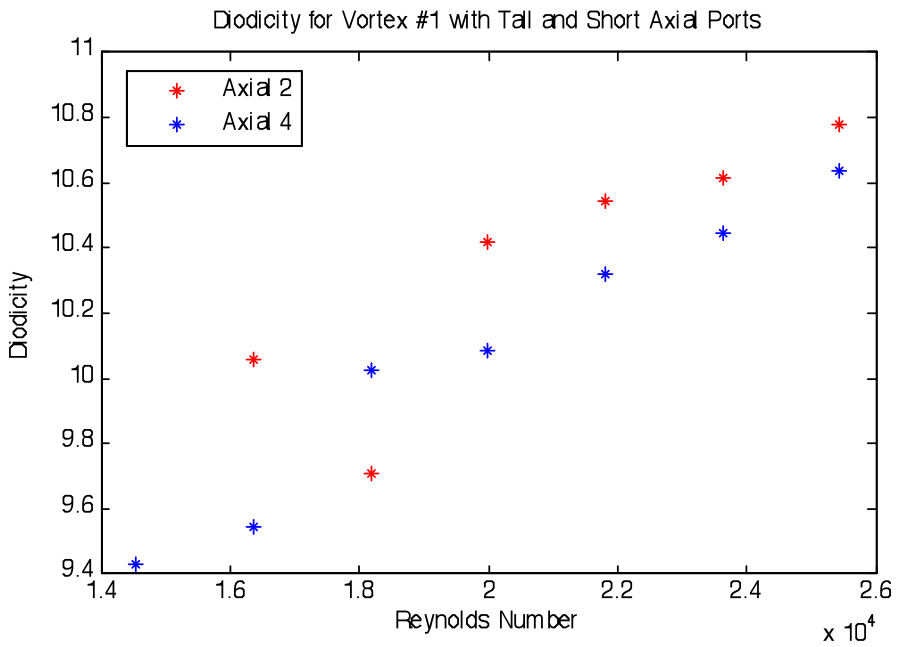

Fig. 5-4 Diodicity with respect to Reynolds number for small diode with axial ports 1 and 4.

From Fig. 5-4 it can be seen that the diodicity for Reynolds numbers from 1.4 – 2.6 x 10^4 is higher for the tall axial port than for the short axial port. This can be explained by the fact that the longer axial port maintains the swirl in the fluid for a greater distance than the shorter port does. This creates a larger pressure drop in the high resistance direction. The slightly increased wall friction in the low resistance direction does not offset this effect.

The last parameter that we varied for the diode was the inlet condition at the tangential port. We did this by using a series of elbows just before the tangential inlet in the high resistance direction to create turbulence. This added turbulence caused the fluid to behave as if it were at higher Reynolds number. There was therefore a higher value of $\Delta \mathbf{P}_H$ with the series of elbows than for the straight pipe section. There would also be a larger value of $\Delta \mathbf{P}_L$, we therefore had to determine the net effect of these increased pressure drops. We compared these diodicities of the small diode using both axial port 1 and axial port 4. We used axial ports 1 and 4 so that we could make a direct comparison between the results and determine if there were separate effects contributing to the increase in diodicity. The plots using these two different axial ports are shown in Figure 5-5 below.

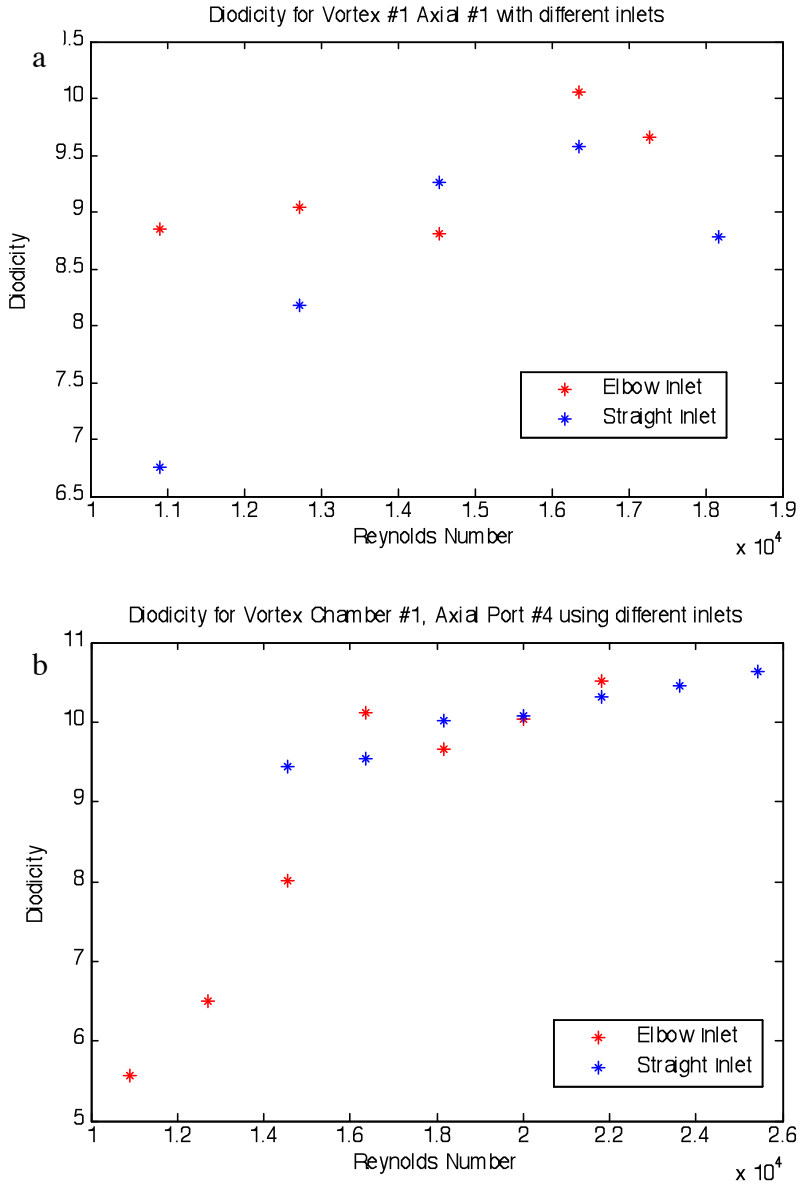

Fig. 5-5 (a) Shows the diodicity with Reynolds number for the elbow inlet and the straight inlet using axial port 1. (b) Shows the diodicity with Reynolds number for the elbow inlet and the straight inlet using axial port 4.

Figure 5-5 show that the series of elbows does increase diodicity with Reynolds numbers in the range of 1.0 -1.9 x 10^4. At this point it can be seen in Figure 5-5 (b) that the diodicity using the straight inlet section starts to become close to or even exceeds the diodicity when using the elbow inlet section. This may be because the Reynolds is high enough to where the turbulence from the elbows no longer increases the effective Reynolds number felt by the fluid. It would then only act as added resistance in the low resistance direction and decrease the diodicity.

5.2 Sources of Uncertainty

There is systematic error associated with reading the measurement tools. The rotameter has divisions of 0.5 gallons per minute (GPM). There is some difficulty in measuring the flow rate with such few divisions. The pressure drops across the diode are sensitive to the flow rate as well, affecting the calculated diodicity.

There also systemic error in reading the manometers. There is about one or two millimeters of error associated with reading the height of the column of water in the manometer tube. The error is relatively small, but the diodicity calculation is sensitive to small changes in the pressure drop across the low-resistance path.

In the high-resistance path, reading pressure from the gauge introduced much larger uncertainties than with the manometers. The smallest unit of measurement on the pressure gauge is 3.45 KPa (0.5) psi, which equates to approximately 39.4 cm of head on the manometers. Therefore we can expect uncertainty on the order of tens of centimeters of head when using the pressure gauge to record measurements.

It was difficult to ensure the system reached steady state equilibrium prior to taking measurements. The water levels changed slowly and it was easy to take measurements before the system achieved equilibrium. In this experiment, we took special care in allowing sufficient time to pass after changing the flow rate as well as monitoring if the levels changed over long time periods in order to minimize this error.

There is also an uncertainty in matching the physical phenomenology of the prototypical system. As the length scale is reduced for the model relative to the prototype, surface roughness distortions become more and more pronounced. The surface finish on the inside of the vortex chamber was achieved by filling rough patches and hand-sanding until it felt smooth to the touch. The surface for the model is not as smooth as the prototypical system, and it is unclear whether or not the surface roughness of the fabricated diodes played a significant role in the diodicity.

6.0 CONCLUSIONS

This design project used an empirical approach to scope the performance of a fluidic diode device. Although the range of Reynolds numbers was limited and the relative diodicity was low, the experiment served as a proof-of-principle study. The project will aid further study into measuring the performance of various fluidic diode assemblies by providing insight for limitations on the experimental range and the accuracy of measurements.

The ease of fabrication for the vortex diode still makes it an attractive candidate for use in PB-AHTR. In this study we have confidence in the ability to fabricate and test scaled fludic diodes while maintaining physical and dynamic similarity to the prototypical system.

6.1 Recommended Future Experiments

From section 5.0, the range of Reynolds number covered was extremely limited. Reynolds numbers near 50,000 need to be investigated in order to make a conclusion for the effectiveness of use in the PB-AHTR. In order to accurately measure pressure drop across the diode at these values, we need a much taller tank for sufficient head to reach steady state flow in the low-resistance path. In addition, our low range of Reynolds was also limited by the physical height of the vortex diode assembly. For any equilibrium height of water below this physical height, we were unable to measure the pressure drop due to the locations of manometer taps. A new experimental setup that addresses these limitations is necessary to inspect a wider range of Reynolds numbers.

The rapid prototyping method that was used for fabricating the vortex chamber left much to be desired in terms of surface roughness. It would be interesting to test a set of vortex chambers with an intentionally roughened surface in order to see how it would affect the diode's performance. It is unclear whether or not surface roughness played a role in the relatively low diodicity values for this experiment.

Although a test for turbulent incoming flow was performed using a series of pipe elbows, fabricating an inlet that induces a swirling flow and seeing the impact on the diodicity is something to be looked at. From this study, the series of elbows increased the performance of the diode assemblies tested, and it would be interesting to see how much a swirler could increase performance.

7.0 REFERENCES

1. A. A. Kulkarni, V. V. Ranade, R. Rajeev, and S. B. Koganti, "CFD Simulation of Flow in Vortex Diodes," *Wiley InterScience*, March, 2008.
2. C.W. Forsberg, D.L. Moses, E.B. Lewis, R. Gibson, R. Pearson, W.J. Reich, G.A. Murphy, R.H. Staunton, W.E. Kohn, "Proposed and Existing Passive and Inherent Safety-Related Structures, Systems, and Components for ALWRs," U.S. Department of Energy Office of Nuclear Energy, October 1989.
3. Rothfuss and F. Vogt, "Reactpr Vessel Technology," Nuclear Technology, Vol. 78, p. 245, 1987.
4. A. A. Kulkarni, V. V. Ranade, R. Rajeev, and S. B. Koganti, "Pressure Drop Across Vortex Diodes: Experiments and Design Guidelines," Chemical Engineering Science, November, 2008.
5. E. Blandford, J. Tang, R. Wang, P. Peterson, "Progress in the Development of the Modular Pebble-Bed Advanced High Temperature Reactor," GLOBAL 2009 Conference, September, 2009.
6. P. Kundu, I. Cohen, P. Ayyaswamy, "Fluid Mechanics," Academic Press, November 2007.

8.0 ACKNOWLEDGEMENTS

This project could not be completed without tremendous support from individuals from the University of California, Berkeley. Special thanks go to Professor Per Peterson and Edward Blandford from the department of Nuclear Engineering. We also thank Mick Franssen, Gordon Long, and Wendy Penning from the Instructional and Technical Support Group for assistance in the fabrication of the diodes.

APPENDIX A: Raw Data Values

Vortex 1, Axial 1, Straight Inlet

GPM	Re Number	ΔP (Forward) [cm of head]	ΔP (Reverse) [cm of head]	Diodicity
3.000	10905	13.97	94.30	6.750
3.500	12723	15.88	129.86	8.180
4.000	14541	20.32	188.12	9.258
4.500	16358	26.51	253.68	9.569
5.000	18176	33.34	292.89	8.786

Vortex 1, Axial 2, Straight Inlet

GPM	Re Number	ΔP (Forward) [cm of head]	ΔP (Reverse) [cm of head]	Diodicity
4.500	16358	10.48	105.41	10.061
5.000	18176	13.49	130.97	9.706
5.500	19993	17.15	178.59	10.417
6.000	21811	20.32	214.25	10.544
6.500	23628	24.61	261.24	10.617
7.000	25446	27.15	292.58	10.778

Vortex 1, Axial 3, Straight Inlet

GPM	Re Number	ΔP (Forward) [cm of head]	ΔP (Reverse) [cm of head]	Diodicity
5.000	18176	9.68	74.77	7.721
5.500	19993	12.22	96.52	7.896
6.000	21811	15.24	116.84	7.667
6.500	23628	17.78	141.92	7.982
7.000	25446	21.11	167.80	7.947

Vortex 1, Axial 4, Straight Inlet

GPM	Re Number	ΔP (Forward) [cm of head]	ΔP (Reverse) [cm of head]	Diodicity
4	14541	8.10	76.36	9.431
4.5	16358	10.48	100.01	9.545
5	18176	13.18	132.08	10.024
5.5	19993	16.99	171.29	10.084
6	21811	20.00	206.38	10.317
6.5	23628	24.13	252.03	10.445

7	25446	27.94	297.21	10.6375

Vortex 1, Axial 1, Elbow Inlet

GPM	Re Number	ΔP (Forward) [cm of head]	ΔP (Reverse) [cm of head]	Diodicity
3	10905	11.59	102.55	8.849
3.5	12723	14.92	134.94	9.043
4	14541	19.69	173.51	8.815
4.5	16358	24.45	245.81	10.055
4.75	17267	28.73	277.30	9.651

Vortex 1, Axial 4, Elbow Inlet

GPM	Re Number	ΔP (Forward) [cm of head]	ΔP (Reverse) [cm of head]	Diodicity
3	10905	7.78	43.34	5.571
3.5	12723	9.05	58.90	6.509
4	14541	10.32	82.71	8.015
4.5	16358	10.64	107.63	10.119
5	18176	13.65	131.76	9.651
5.5	19993	16.51	165.58	10.029
6	21811	20.00	210.19	10.508

Vortex 2, Axial 2, Straight Inlet

GPM	Re Number	ΔP (Forward) [cm of head]	ΔP (Reverse) [cm of head]	Diodicity
4.5	16358	12.54	97.47	7.772
5	18176	14.92	126.68	8.489
5.5	19993	18.89	157.48	8.336
6	21811	18.26	190.02	10.409
6.5	23628	21.43	223.84	10.444
7	25446	24.92	250.13	10.036

Vortex 3, Axial 2, Straight Inlet

GPM	Re Number	ΔP (Forward) [cm of head]	ΔP (Reverse) [cm of head]	Diodicity
5	18176	11.91	91.60	7.693
5.5	19993	14.61	117.32	8.033
6	21811	18.10	146.37	8.088
6.5	23628	21.11	170.82	8.090
7	25446	24.13	202.09	8.375

Appendix B: Design Schematics

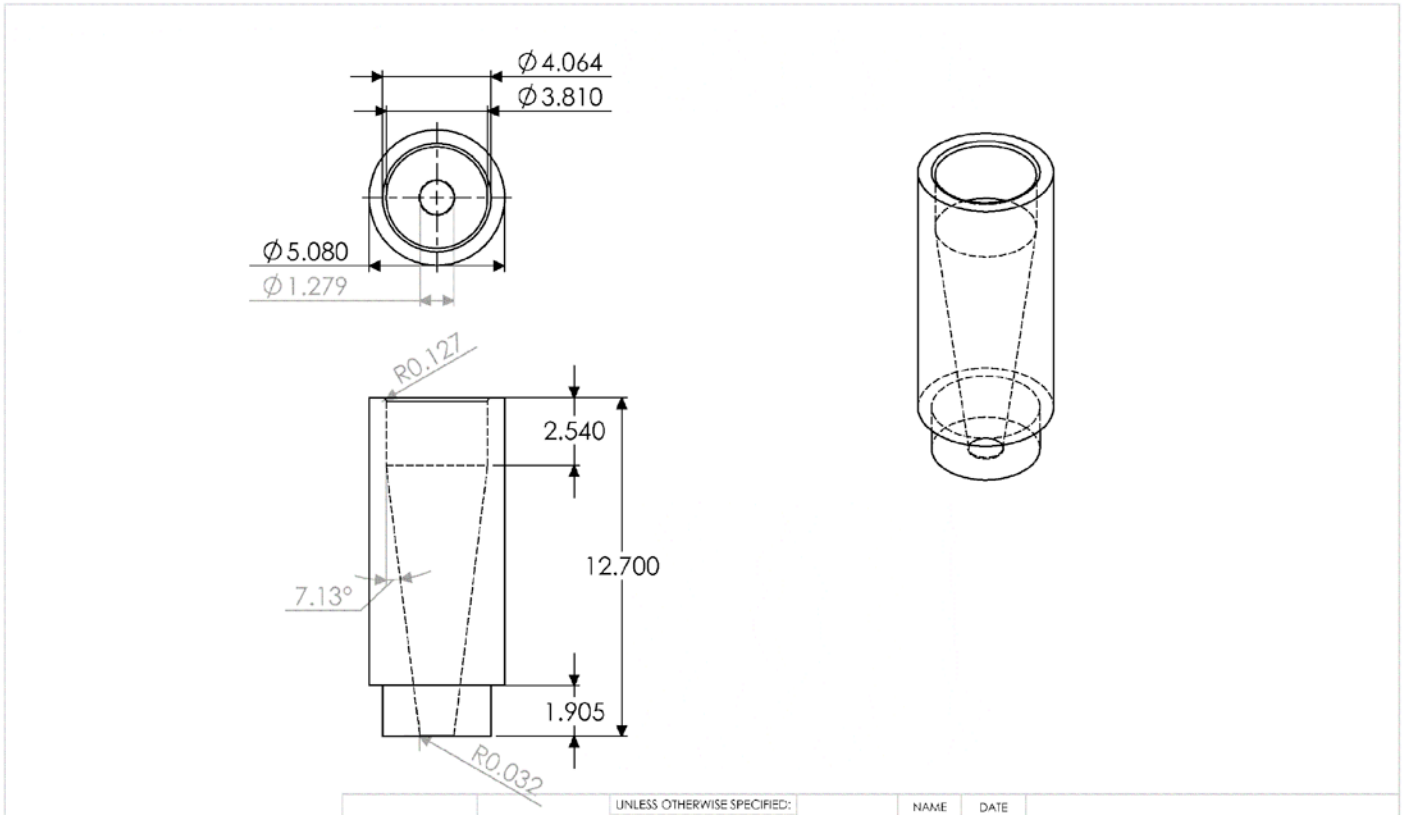

		UNLESS OTHERWISE SPECIFIED:		NAME	DATE
		DIMENSIONS ARE IN CM TOLERANCES: FRACTIONAL ± ANGULAR: MACH ± BEND ± TWO PLACE DECIMAL ± THREE PLACE DECIMAL ±	DRAWN		
			CHECKED		
			ENG APPR.		
			MFG APPR.		
		INTERPRET GEOMETRIC TOLERANCING PER:	Q.A.		
		MATERIAL	COMMENTS:		
NEXT ASSY	USED ON	FINISH			
APPLICATION		DO NOT SCALE DRAWING			

PROPRIETARY AND CONFIDENTIAL

THE INFORMATION CONTAINED IN THIS DRAWING IS THE SOLE PROPERTY OF <INSERT COMPANY NAME HERE>. ANY REPRODUCTION IN PART OR AS A WHOLE WITHOUT THE WRITTEN PERMISSION OF <INSERT COMPANY NAME HERE> IS PROHIBITED.

TITLE:

Axial Port #1

SIZE	DWG. NO.	REV
A		
SCALE: 1:2	WEIGHT:	SHEET 1 OF 1

5 4 3 2 1

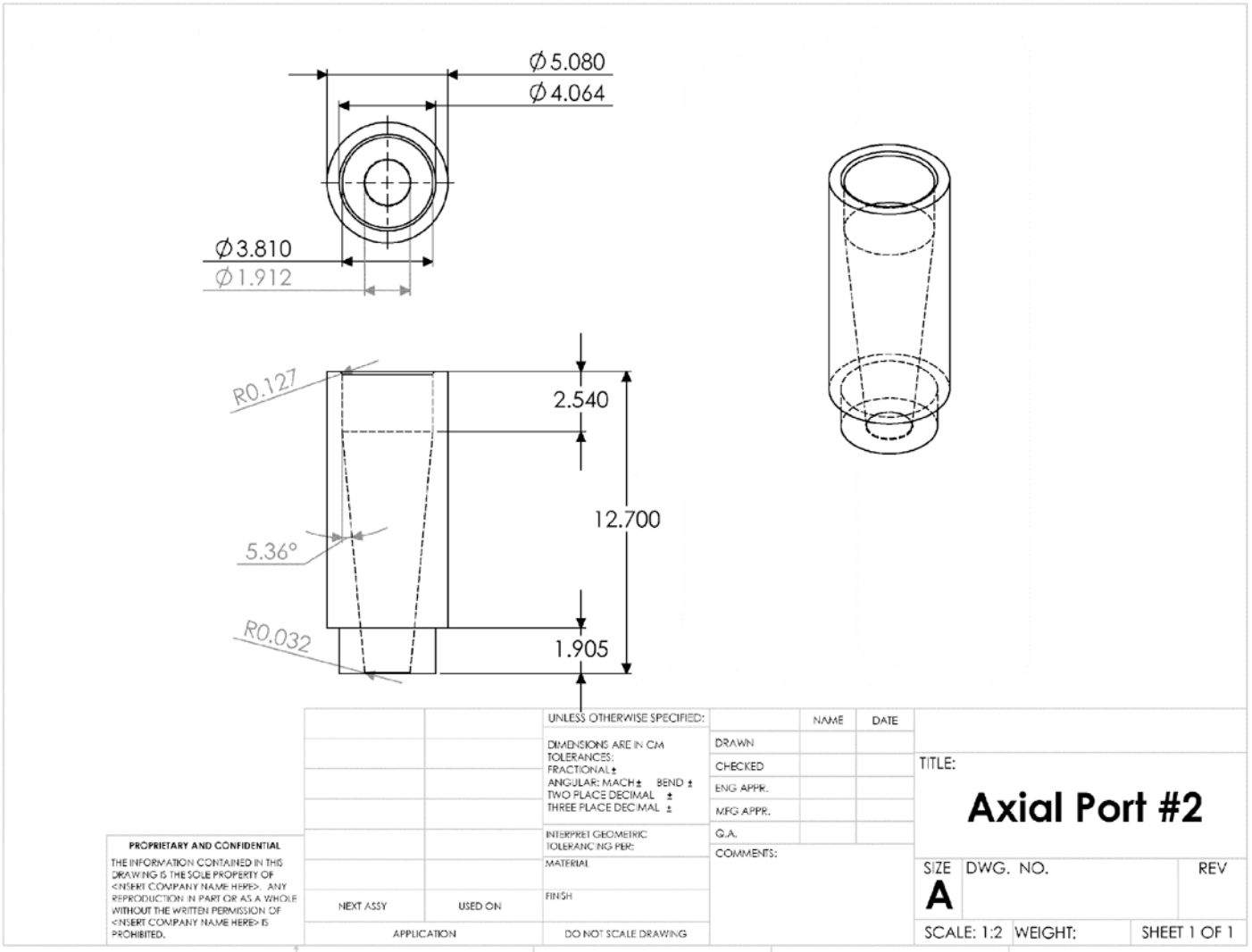
Ø5.080
Ø4.064
Ø3.810
Ø1.912
R0.127
2.540
12.700
5.36°
R0.032
1.905
UNLESS OTHERWISE SPECIFIED:
DIMENSIONS ARE IN CM
TOLERANCES:
FRACTIONAL ±
ANGULAR: MACH ± BEND ±
TWO PLACE DECIMAL ±
THREE PLACE DECIMAL ±
INTERPRET GEOMETRIC TOLERANCING PER:
MATERIAL
FINISH
NEXT ASSY
USED ON
APPLICATION
DO NOT SCALE DRAWING
NAME
DATE
DRAWN
CHECKED
ENG APPR.
MFG APPR.
G.A.
COMMENTS:
PROPRIETARY AND CONFIDENTIAL
THE INFORMATION CONTAINED IN THIS DRAWING IS THE SOLE PROPERTY OF <INSERT COMPANY NAME HERE>. ANY REPRODUCTION IN PART OR AS A WHOLE WITHOUT THE WRITTEN PERMISSION OF <INSERT COMPANY NAME HERE> IS PROHIBITED.
TITLE:
Axial Port #2
SIZE
A
DWG. NO.
REV
SCALE: 1:2
WEIGHT:
SHEET 1 OF 1
5
4
3
2
1

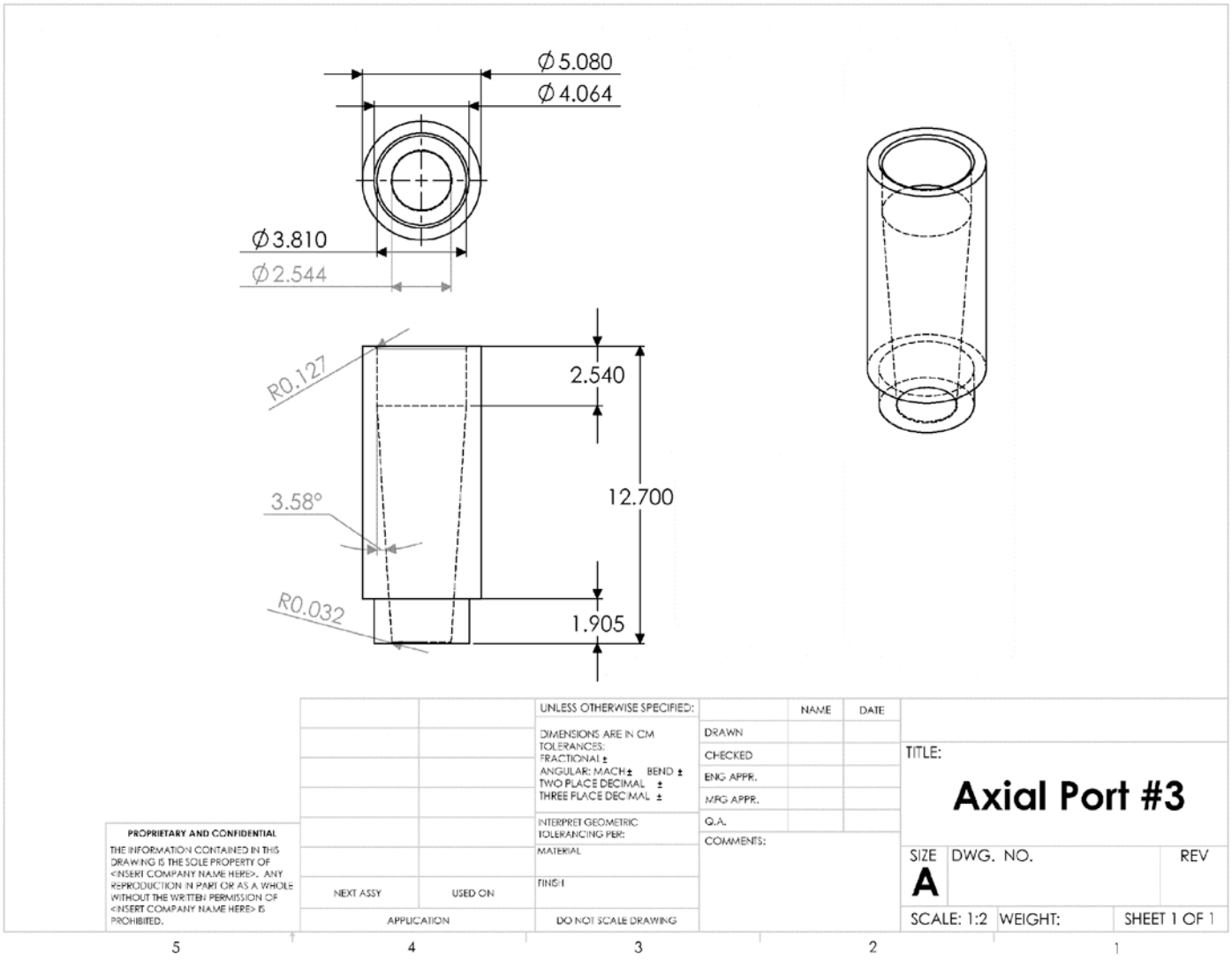
Ø5.080
Ø4.064
Ø3.810
Ø2.544
R0.127
2.540
12.700
3.58°
R0.032
1.905
UNLESS OTHERWISE SPECIFIED:
DIMENSIONS ARE IN CM
TOLERANCES:
FRACTIONAL ±
ANGULAR: MACH ± BEND ±
TWO PLACE DECIMAL ±
THREE PLACE DECIMAL ±
INTERPRET GEOMETRIC TOLERANCING PER:
MATERIAL
FINISH
NEXT ASSY
USED ON
APPLICATION
DO NOT SCALE DRAWING
NAME
DATE
DRAWN
CHECKED
ENG APPR.
MFG APPR.
Q.A.
COMMENTS:
PROPRIETARY AND CONFIDENTIAL
THE INFORMATION CONTAINED IN THIS DRAWING IS THE SOLE PROPERTY OF <INSERT COMPANY NAME HERE>. ANY REPRODUCTION IN PART OR AS A WHOLE WITHOUT THE WRITTEN PERMISSION OF <INSERT COMPANY NAME HERE> IS PROHIBITED.
TITLE:
Axial Port #3
SIZE
A
DWG. NO.
REV
SCALE: 1:2
WEIGHT:
SHEET 1 OF 1
5
4
3
2
1

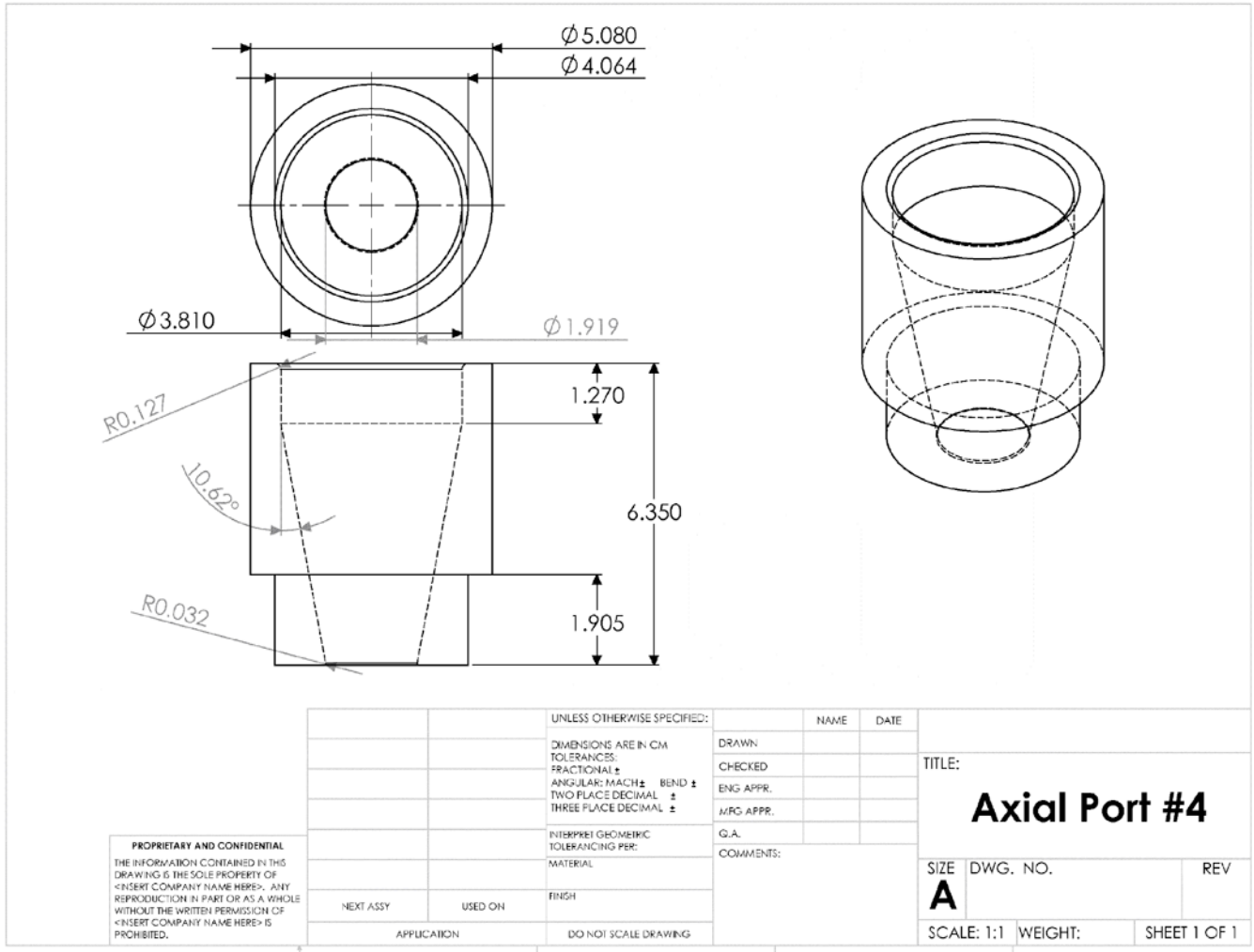
Ø5.080
Ø4.064
Ø3.810
Ø1.919
R0.127
10.62°
1.270
6.350
R0.032
1.905
UNLESS OTHERWISE SPECIFIED:
DIMENSIONS ARE IN CM
TOLERANCES:
FRACTIONAL ±
ANGULAR: MACH ± BEND ±
TWO PLACE DECIMAL ±
THREE PLACE DECIMAL ±
INTERPRET GEOMETRIC TOLERANCING PER:
MATERIAL
FINISH
NEXT ASSY
USED ON
APPLICATION
DO NOT SCALE DRAWING
NAME
DATE
DRAWN
CHECKED
ENG APPR.
MFG APPR.
G.A.
COMMENTS:
PROPRIETARY AND CONFIDENTIAL
THE INFORMATION CONTAINED IN THIS DRAWING IS THE SOLE PROPERTY OF <INSERT COMPANY NAME HERE>. ANY REPRODUCTION IN PART OR AS A WHOLE WITHOUT THE WRITTEN PERMISSION OF <INSERT COMPANY NAME HERE> IS PROHIBITED.
TITLE:
Axial Port #4
SIZE
A
DWG. NO.
REV
SCALE: 1:1
WEIGHT:
SHEET 1 OF 1
5
4
3
2
1

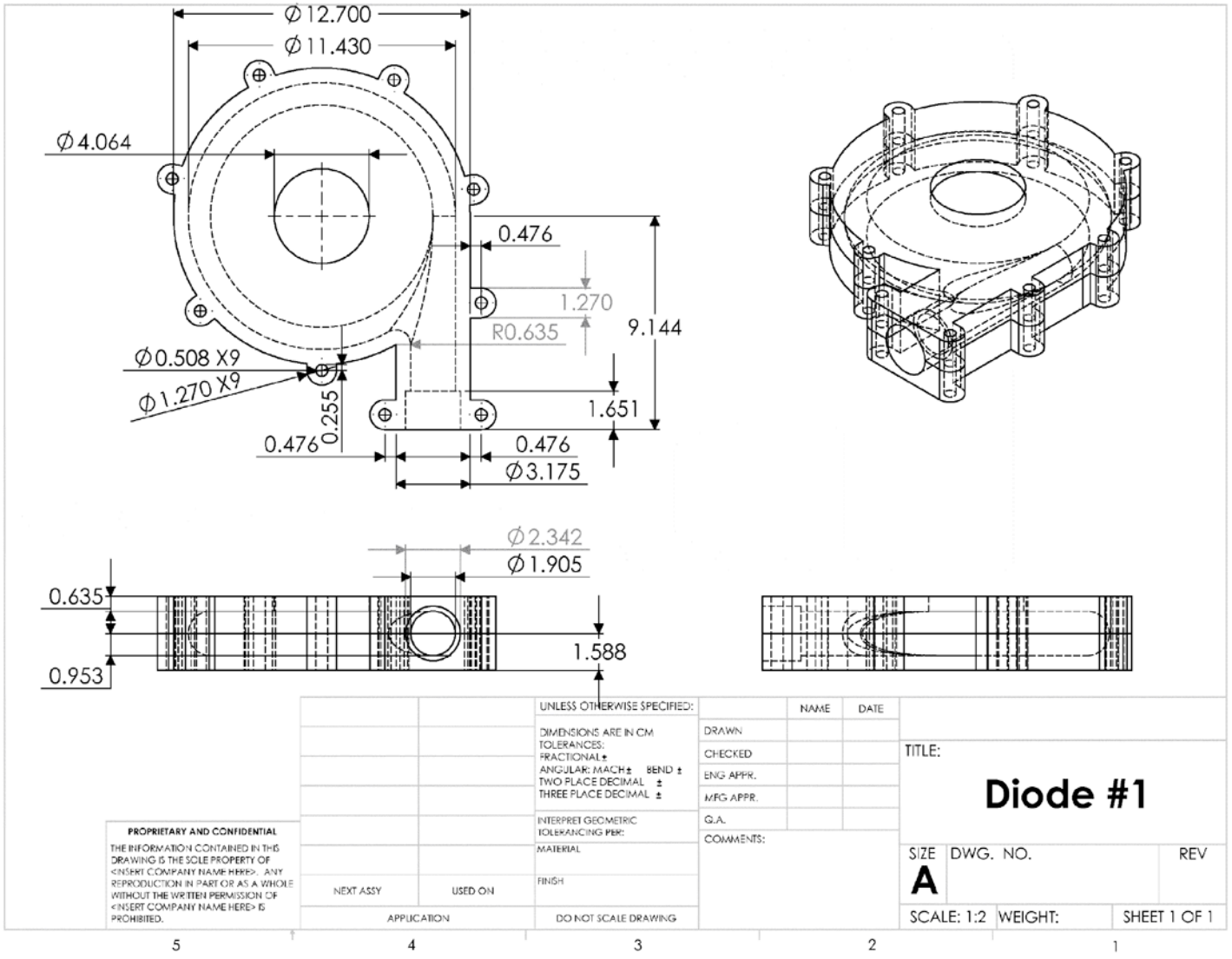
Ø12.700
Ø11.430
Ø4.064
0.476
1.270
R0.635
9.144
Ø0.508 X9
Ø1.270 X9
0.255
1.651
0.476
0.476
Ø3.175
Ø2.342
Ø1.905
0.635
0.953
1.588
UNLESS OTHERWISE SPECIFIED:
DIMENSIONS ARE IN CM
TOLERANCES:
FRACTIONAL ±
ANGULAR: MACH ± BEND ±
TWO PLACE DECIMAL ±
THREE PLACE DECIMAL ±
INTERPRET GEOMETRIC TOLERANCING PER:
MATERIAL
FINISH
NEXT ASSY
USED ON
APPLICATION
DO NOT SCALE DRAWING
NAME
DATE
DRAWN
CHECKED
ENG APPR.
MFG APPR.
Q.A.
COMMENTS:
PROPRIETARY AND CONFIDENTIAL
THE INFORMATION CONTAINED IN THIS DRAWING IS THE SOLE PROPERTY OF <INSERT COMPANY NAME HERE>. ANY REPRODUCTION IN PART OR AS A WHOLE WITHOUT THE WRITTEN PERMISSION OF <INSERT COMPANY NAME HERE> IS PROHIBITED.
TITLE:
Diode #1
SIZE
A
DWG. NO.
REV
SCALE: 1:2
WEIGHT:
SHEET 1 OF 1
5
4
3
2
1

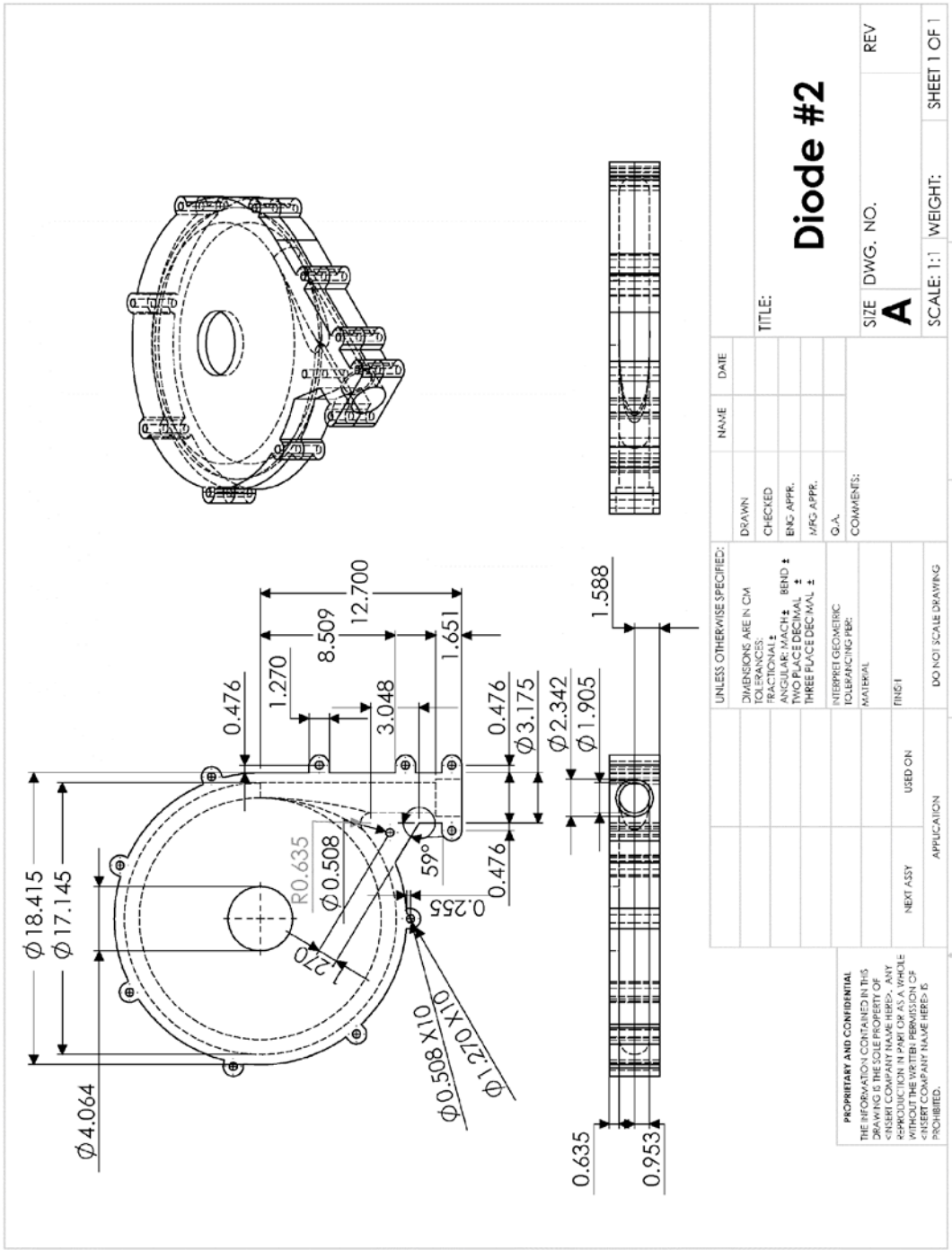
Diode #2
SIZE A
DWG. NO.
REV
SCALE: 1:1
WEIGHT:
SHEET 1 OF 1
TITLE:
UNLESS OTHERWISE SPECIFIED:
DRAWN
CHECKED
ENG APPR.
MFG APPR.
Q.A.
COMMENTS:
NAME
DATE
DIMENSIONS ARE IN CM
TOLERANCES:
FRACTIONAL ±
ANGULAR: MACH ± BEND ±
TWO PLACE DECIMAL ±
THREE PLACE DECIMAL ±
INTERPRET GEOMETRIC TOLERANCING PER:
MATERIAL
FINISH
NEXT ASSY
USED ON
APPLICATION
DO NOT SCALE DRAWING
PROPRIETARY AND CONFIDENTIAL
THE INFORMATION CONTAINED IN THIS DRAWING IS THE SOLE PROPERTY OF <INSERT COMPANY NAME HERE>. ANY REPRODUCTION IN PART OR AS A WHOLE WITHOUT THE WRITTEN PERMISSION OF <INSERT COMPANY NAME HERE> IS PROHIBITED.
ϕ18.415
ϕ17.145
ϕ4.064
0.476
1.270
8.509
12.700
3.048
1.651
0.476
ϕ3.175
ϕ2.342
ϕ1.905
1.588
R0.635
ϕ0.508
59°
0.255
0.476
1.270
ϕ0.508 X10
ϕ1.270 X10
0.635
0.953

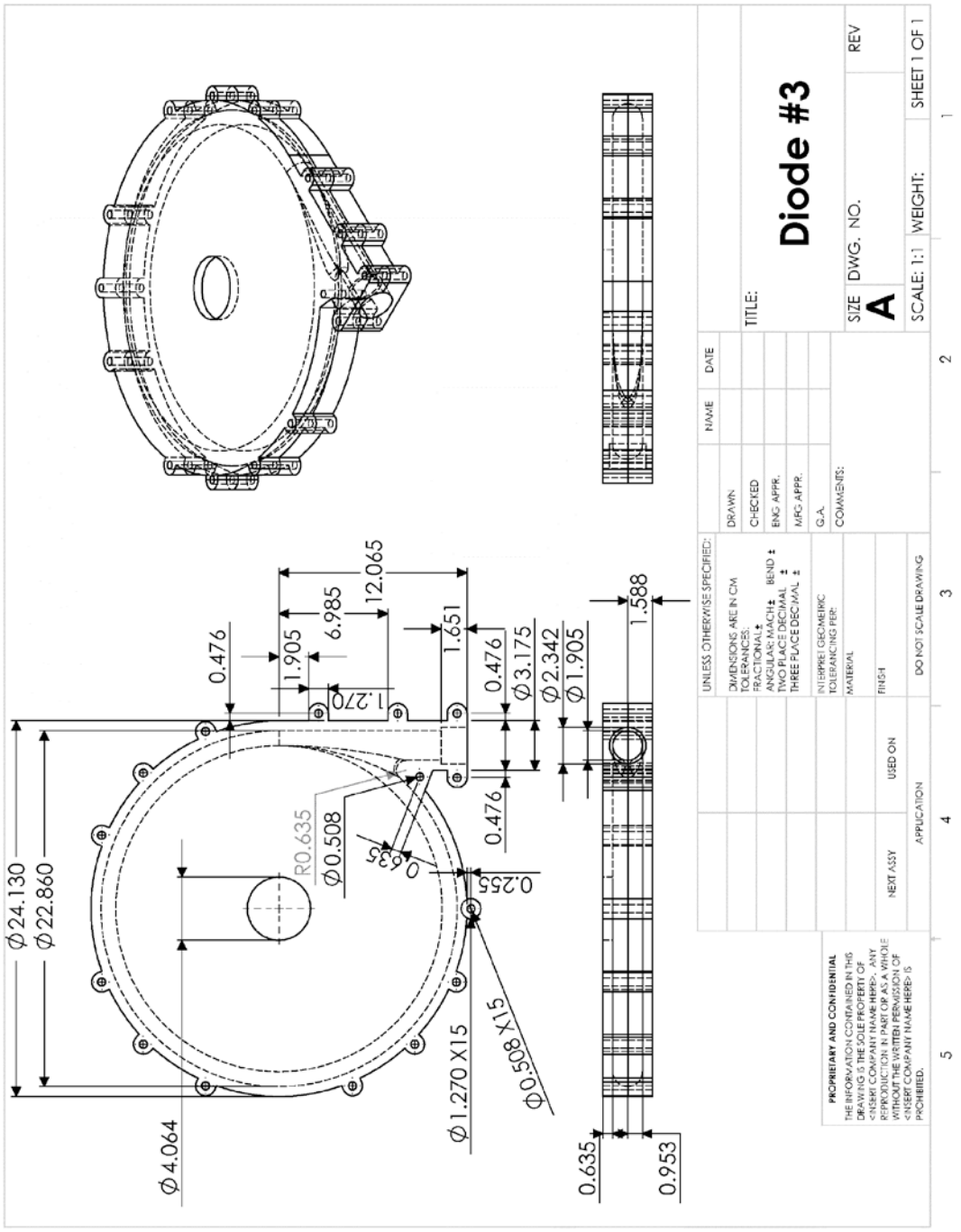
Diode #3
SIZE A
DWG. NO.
REV
SCALE: 1:1
WEIGHT:
SHEET 1 OF 1
TITLE:
UNLESS OTHERWISE SPECIFIED:
DRAWN
CHECKED
ENG APPR.
MFG APPR.
Q.A.
COMMENTS:
NAME
DATE
MATERIAL
FINISH
NEXT ASSY
USED ON
APPLICATION
DO NOT SCALE DRAWING
PROPRIETARY AND CONFIDENTIAL
Φ24.130
Φ22.860
Φ4.064
0.476
1.905
6.985
12.065
1.270
1.651
0.476
Φ3.175
Φ2.342
Φ1.905
1.588
R0.635
Φ0.508
0.635
0.255
0.476
Φ1.270 X15
Φ0.508 X15
0.635
0.953

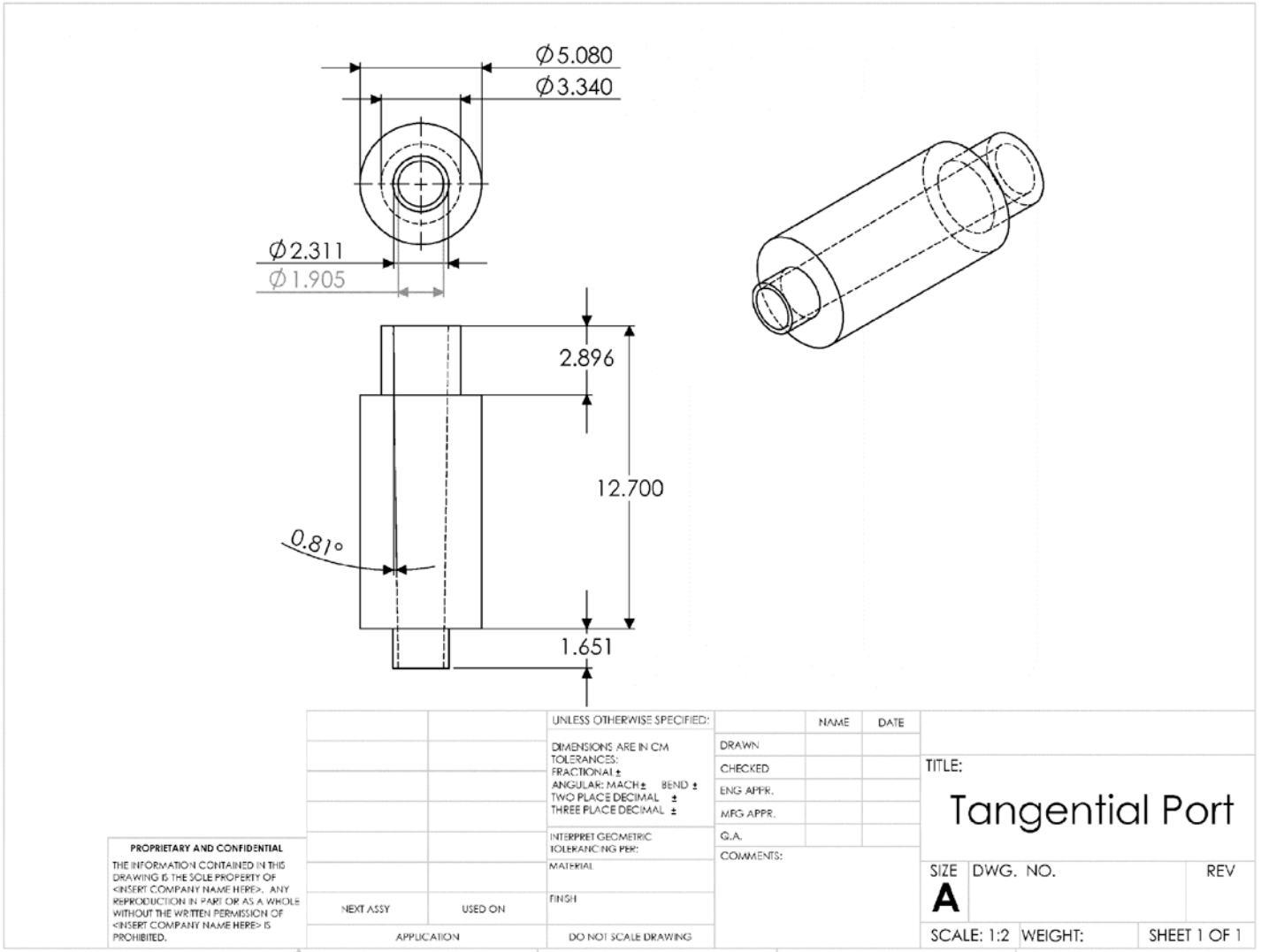
Ø5.080
Ø3.340
Ø2.311
Ø1.905
2.896
12.700
0.81°
1.651
UNLESS OTHERWISE SPECIFIED:
DIMENSIONS ARE IN CM
TOLERANCES:
FRACTIONAL ±
ANGULAR: MACH ± BEND ±
TWO PLACE DECIMAL ±
THREE PLACE DECIMAL ±
INTERPRET GEOMETRIC TOLERANCING PER:
MATERIAL
FINISH
NEXT ASSY
USED ON
APPLICATION
DO NOT SCALE DRAWING
NAME
DATE
DRAWN
CHECKED
ENG APPR.
MFG APPR.
G.A.
COMMENTS:
PROPRIETARY AND CONFIDENTIAL
THE INFORMATION CONTAINED IN THIS DRAWING IS THE SOLE PROPERTY OF <INSERT COMPANY NAME HERE>. ANY REPRODUCTION IN PART OR AS A WHOLE WITHOUT THE WRITTEN PERMISSION OF <INSERT COMPANY NAME HERE> IS PROHIBITED.
TITLE:
Tangential Port
SIZE
A
DWG. NO.
REV
SCALE: 1:2
WEIGHT:
SHEET 1 OF 1
5
4
3
2
1

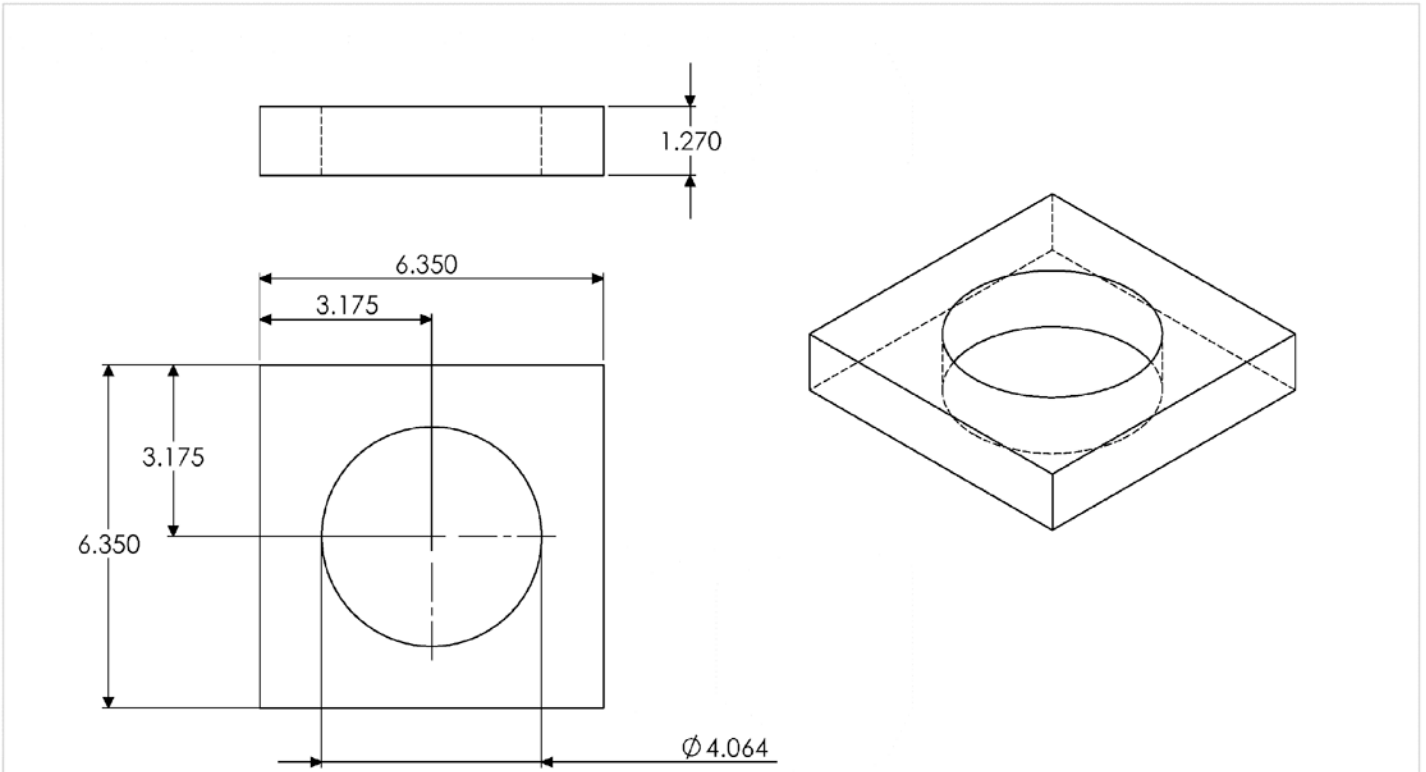

		UNLESS OTHERWISE SPECIFIED:		NAME	DATE
		DIMENSIONS ARE IN CM TOLERANCES: FRACTIONAL ± ANGULAR: MACH ± BEND ± TWO PLACE DECIMAL ± THREE PLACE DECIMAL ±	DRAWN		
			CHECKED		
			ENG APPR.		
			MFG APPR.		
		INTERPRET GEOMETRIC TOLERANCING PER:	Q.A.		
		MATERIAL	COMMENTS:		
NEXT ASSY	USED ON	FINISH			
APPLICATION		DO NOT SCALE DRAWING			

PROPRIETARY AND CONFIDENTIAL

THE INFORMATION CONTAINED IN THIS DRAWING IS THE SOLE PROPERTY OF <INSERT COMPANY NAME HERE>. ANY REPRODUCTION IN PART OR AS A WHOLE WITHOUT THE WRITTEN PERMISSION OF <INSERT COMPANY NAME HERE> IS PROHIBITED.

TITLE:

Spacer

SIZE	DWG. NO.	REV
A		
SCALE: 1:1	WEIGHT:	SHEET 1 OF 1

5 4 3 2 1